# Dynamic Modelling and Control Strategy of a Temperature-Driven Metal Hydride Cooling System for Buildings

**Saket Verma *[a,c], Ravi Anant Kishore [b], Kuldeep Kumar [c,d] & Pratheek Ranjan Mitra [a]**

[a] Department of Mechanical Engineering, Birla Institute of Technology and Science, Pilani, Pilani Campus, Vidya Vihar, Rajasthan 333 031, India.

[b] National Renewable Energy Laboratory, 15013 Denver West Pkwy, Golden, CO 80401, USA

[c] School of Energy Science and Engineering, Indian Institute of Technology Guwahati 781039, Assam, India

[d] School of Electrical, Computer and Telecommunications Engineering, University of Wollongong, Northfields Ave Wollongong, NSW 2522 Australia

* Corresponding author

E-mail address: saketverma@hotmail.com (Saket Verma).

## Abstract

A temperature-driven coupled metal hydride (MH) based thermal energy storage (TES) system can allow to shave and shift the peak energy demand in buildings. The high energy density and long-term (seasonal) energy storage capability are its major advantages over other energy storage methods. The dynamic nature of the MH operation, however, requires controlled hydrogen transfer between the coupled MHs at a rate needed to meet the building's transient load. While temperature-driven MH systems are studied in the literature, their application in buildings and control are scarcely reported. This paper presents a control-based dynamic modeling of the temperature-driven coupled MH-TES system for building cooling applications. The dynamic model is developed in MATLAB® Simulink environment, considering the thermodynamic and kinetic behaviors of the MH systems. Based on a preliminary analysis of a property database of over 337 hydrides, we select around 1600 MH pairs suitable for building cooling applications. Each of these MH pairs is studied for their performance using the dynamic model, and among all, $Zr_{0.76}Ti_{0.24}Ni_{1.16}Mn_{0.63}V_{0.14}Fe_{0.18}$–$Ti_{0.85}Zr_{0.15}Cr_{1.2}Mn_{0.8}$ MH pair showed fast dynamics along with high coefficient of performance (COP) of 0.71. A parametric investigation is performed on this MH pair to understand the effect of operating temperatures. Finally, three proportional-integral (PI) feedback controllers are investigated to regulate the temperature, pressure and mass exchange between the coupled MH pairs. The developed PI controller is sufficiently capable of rejecting the signal noise from the hydrogen flow and internal heat exchange processes with root mean square error of 5.78 W between reference and actual cooling load.

**Keywords:** Building cooling; Control systems, Dynamic Model; Hydrogen storage; Metal hydride; Thermal energy storage

## 1. Introduction

The time imbalance between peak energy demand and peak energy production is becoming increasingly significant with increasing contributions of renewable energy in the total energy generation mix making energy storage a crucial technology for clean energy deployment. The energy can be stored in the form of high-grade energy such as electrical energy storage (EES) and mechanical energy storage (MES), or low-grade energy such as thermal energy storage (TES), chemical energy storage (CES), thermochemical energy storage (TCES), electrochemical energy storage (ECES), etc. Energy storage in the form of high-grade energy is particularly important as well as challenging for grid and microgrid levels, and also with long cycle times. Electrical batteries are currently the most common technology used for storing electricity; however, TES is the preferred option in building applications, particularly for space heating and cooling [1], because a significant portion of the energy used in buildings is related to thermal load [2]. The key benefits of TES are related to cost savings, load shifting, load shaving, and matching demand and supply of energy [3, 4]. The two commonly used TES technologies in buildings are sensible heat storage (SHS) and latent heat storage (LHS) [5]. As the name suggests, SHS technology exploits the high specific heat, whereas LHS technology uses the phase change enthalpy of a suitably selected material to store the thermal energy. However, both technologies have an inherent disadvantage of heat leakage due to which long-term energy storage becomes inefficient [5]. This issue can be addressed by thermochemical energy storage (TCES) [5], which relies on chemical reactions to achieve the same goal. Since energy is stored in the form of chemical bonds rather than heat, it can be stored for longer durations with minor losses. Furthermore, TCES systems offer high energy storage density as compared to both SHS and LHS technologies [1].

Metal hydrides (MH) have attracted great attention recently as a promising TCES medium. MH-based TES is achieved due to the reversible chemical reactions of hydrogen with a metal or intermetallic alloy at a certain temperature and pressure [6]. Compared to latent or sensible heat storage options, MH-based TES has the advantages of much higher energy densities (0.5 - 3 GJ/$m^3$), higher cycle efficiency, minimal losses, and reversibility [7]. The long-term (seasonal) energy storage capability of MHs offers the required load flexibility for heating/cooling applications. A comparison between metal hydride (MH) and phase change material (PCM) based thermal energy storage for building applications is given in Table A.1. In building applications, MH-based energy storage can be used with solar/waste heat as a standalone or integrated system with conventional heating/cooling systems [8]. In the standalone mode, MH-based system works similar to a heat driven refrigerator/heat pump. It can use the available (solar/waste) heat to storage the energy in the form of chemical energy of hydrides. In the later stage, the stored chemical energy is converted into heating/cooling effect, and delivered to the building using a suitable working fluid that transfers heat between MH and building heat exchangers [9]. In the integrated mode, MH-based energy storage can be appropriately sized to work in combination with a conventional heating, ventilation and air-conditioning (HVAC) system, where it can be used for peak load shaving. In such an integrated system, the excess (solar/waste heat) energy or cheap electricity can be used to store the energy with MH. In the peak load hours, the MH system works along with the conventional HVAC

system to supply heating/cooling effect, which allows for the downsizing of conventional HVAC system. The MH system can use the same or different working fluid as that of the conventional HVAC system, which exchanges heat with the building air-heat exchanger to provide heating/cooling effect [10].

## 2. Literature review

MH-TES systems can be categorized as either heat-driven systems or compressor-driven systems based on the primary driving force for hydrogen absorption and desorption. Heat-driven hydrides rely on temperature changes, while compression-driven hydrides rely on pressure changes [1]. Recently, heat-driven MH-based TES has been studied widely for concentrated solar power (CSP) plants, where a Rankine cycle is used for electricity generation. The stored solar energy in the MH-based TES system during the daytime is utilized at the nighttime for the uninterrupted operation of steam production and power plants [11]. For such a TES, a pair of MHs is required to mutually transfer hydrogen during charging and discharging cycles. Typically, one of the MHs needs to operate at a high equilibrium temperature (higher than the steam generation temperature), while the other needs to operate at a low equilibrium temperature (lower than the heat sink temperature). The formation of a hydride (absorption/charging cycle) is an exothermic reaction as the entropy of the hydride is reduced compared to the metal and the gaseous hydrogen together. On the other hand, the reverse reaction of the hydrogen desorption process (discharging cycle) is correspondingly endothermic [12]. During the daytime, with the availability of solar energy, the high-temperature metal hydride (HTMH) receives heat and releases hydrogen that is absorbed by the low-temperature metal hydride (LTMH). Likewise, during the nighttime, LTMH releases hydrogen that is absorbed by the HTMH, and heating is produced [1]. Nonetheless, the movement of hydrogen without an external compressor can solely rely on a pressure differential between the two hydrides. This necessitates that the equilibrium pressures of the MHs are appropriately balanced to enable sufficient pressure difference for continuous operation during the charging and discharging processes [13]. Such a coupled MH-based TES system can be configured in many forms, which results into some of the popular applications such as refrigeration system [13,14,15], heat transformers [16,17], and heat pumps [18,19].

Many accounts of theoretical and experimental studies on MH applications specifically for heating and cooling purposes are available in the literature. In one of the earliest attempts during the 1980s, Gruen et al. [20] at Argonne National Laboratory developed an MH-based chemical heat pump that could use solar or other low-grade heat sources. Using $LaNi_5$ and $CaNi_5$ as the MH pair, the cooling capacity of the heat pump was measured as 15,000 kJ/hr when operated with heat input at 117°C, heat rejection at 40°C, and refrigeration taking place at 8°C. This system showed coefficient of performance (COP) of 0.95 with cycle time of 4 minutes. Later, many investigations were performed using MH systems for space conditioning applications. Ron [21] developed a 1 kW air-conditioning system using $LaNi_{4.7}Al_{0.3}$ and $MmNi_{4.15}Fe_{0.85}$ MH pair. He applied this system in a bus, where energy source was the hot exhaust gases from the engine. The maximum specific cooling power of 680 - 900 W/kg of the desorbing hydride was obtained with a cooling time of 2 minutes; however, during the cyclic

operation, the rate of desorption decreased to 200 - 240 W/kg of the desorbing hydride for a complete cycle of 6 minutes. Therefore, it was suggested that suitable MH alloys should be selected to increase the cooling power up to 1 kW/kg so that the MH cooling system can be competitive with the conventional air-conditioners. Similarly, Golben & Huston [22] developed a 2.3 kW cooling capacity air conditioner for an army shelter using $LaNi_{4.5}Al_{0.5}$ as HTMH and (CFM)$Ni_5$ as LTMH alloys. The main purpose of the MH based air-conditioner was to evaluate its suitability as an alternative to electricity driven conventional air-conditioners. Nevertheless, many attempts have been reported in the literature to improve the cooling power and design of the MH-based cooling system, with key achievements in the past few years. Weckerle et al. [23] experimentally demonstrated the possibility of achieving extremely short half-cycle durations ($t < 60$ s), allowing for the creation of compact systems. When considering the utilization of an open MH (Hydralloy® C5) cooling system in a fuel cell vehicle, individual reactor trials displayed a noteworthy cooling capability of 1.3 $kW/kg_{MH}$ at the cooling temperature of 10°C. However, full-cycle operation showed net cooling power of 0.69 $kW/kg_{MH}$, which shows the need for further improvements using reactor design, and reduced parasitic thermal losses. Chandrakala et al. [24] studied La and Mm-based hydrides for cold storage applications. Among various materials tested for cold storage of 10 kg apples at 2°C, $La_{0.95}Ce_{0.05}Ni_5/LaNi_{4.7}Al_{0.3}$ exhibited the highest COP of 0.693, and required the least amount (18.35 kg) of material. The study showed that Mm-based alloys (LTMH) were able to achieve lower cooling temperatures compared to La-based alloys (LTMH). Another important aspect is the degradation of MHs used in thermodynamic machines, which is influenced by various factors, including elevated temperatures, impure hydrogen, and prolonged cycling [25]. These factors can lead to changes in crystal structure, plateau pressure, slope, hysteresis, and reversible hydrogen capacity. Understanding these mechanisms is crucial for designing MH thermal machines with extended service life.

The primary focus of research on MH-based heating and cooling systems has been centered around the design of novel reactors, improving the speed of the reaction, selecting appropriate MH alloy pairs, and conducting experimental tests to assess real-world performance [26]. However, applications of MH in building thermal management are relatively less studied in the literature. Gkanas et al. [27] performed a numerical optimization study for the thickness of different MHs for green building applications. In their study, $AB_2$-based intermetallic MH showed the fastest kinetics compared to $AB_5$-based intermetallics, and therefore, $AB_2$-based intermetallic was the recommended MH for building applications. Kumar et al. [9] performed a model-based investigation on building heating and cooling systems using an MH pair ($Zr_{0.82}Mm_{0.09}Ti_{0.09}Fe_{1.4}Cr_{0.6}$ - $LaNi_{4.6}Al_{0.4}$) and found that the system performance can be controlled by the fraction of the plateau region reacted in the MH pair. Furthermore, the ratio of the mass of MHs for the maximum COP was found at 1.83. Tange et al. [28] demonstrated the feasibility of a hydrogen-based energy storage system for the load leveling of electricity in commercial buildings. Their system utilized an MH tank for on-site storage of hydrogen and its reaction is used for heating/cooling the building. In a 24-hour cycle experiment, it was shown that the system can recover 43.2% thermal energy from the hydrogen storage system. Krane et al. [10] performed a model-based investigation of utilizing MH-coupled heat pump systems for residential heating and cooling purposes. It was found that

while this system demonstrates the ability to manage heating and cooling demands effectively, it only leads to minimal cost reductions. Even under favorable utility rates, the return on investment takes more than 35 years, primarily due to the significant expense associated with MH and hydrogen compressors. It shows that finding a better MH pair that could eliminate the need for a hydrogen compressor is crucial for practical deployment. Zhong and Glanville [29] have highlighted low COP and specific cooling power as the main technical barriers for MH-based thermal systems in building applications. It was also mentioned that total cooling/heating hours are the main parameters determining the payback period for such systems, and the niche markets such as coastal regions could be particularly beneficial by such technology.

The dynamic operation of MH systems requires a suitably designed controller that can provide the requested system outputs. Many studies in literature focus on the dynamic modeling of MH thermal systems; however, only a few of them study their control. Paya et al. [30] developed a dynamic model of the thermal-driven MH cooling system, which was experimentally validated using the MH alloy pair of $LmNi_{4.91}Sn_{0.15}$ and $Ti_{0.99}Zr_{0.01}V_{0.43}Fe_{0.09}Cr_{0.05}Mn_{1.5}$. They found that their MH system provided the mean gravimetric cooling power of 303 W/kg, mean volumetric cooling power of 173 W/L, and COP of around 0.22. Later, Paya et al. [31] presented the optimized performance of MH pairs using numerical and experimental investigations, where it was reported that in addition to the choice of MH pairs, the operating conditions, such as hydrogen charge and cycle duration, significantly influenced the cooling power. Satheesh et al. [32] developed a finite element-based model to study the dynamic behavior of $MmNi_{4.6}Al_{0.4}$ - $MmNi_{4.6}Fe_{0.4}$ MH pair heat pump. The model results suggested that the actual dynamic operations of the MH system deviated from the ideal Van't Hoff plot. Furthermore, the condition of variable wall temperature affected the cycle time, which was found to be delayed. Mellouli et al. [33] developed a thermodynamic model of a dual-bed MH cooling system and presented the results of their parametric study. It was reported that design optimization was critical to achieving high performance from these systems. In their study, an average COP of 0.45 – 0.50 was reported for MH cooling systems that were comparable to heat-driven refrigeration systems such as LiBr-water solar systems. Nyamsi and Tolj [34] developed a 2D numerical model to study the TES performance of a two-tank MH system under both active heat transfer methods, such as forced convection and passive heat transfer methods, such as natural convection, utilizing a phase change material (PCM) with enhanced thermal conductivity. The findings revealed that employing forced convection in a TES system yields superior power output but sacrifices on energy storage efficiency, as some of the stored energy is consumed to enhance the heat transfer within the system. Nonetheless, it was advised to implement thermal conductivity enhancement as it outperformed other passive methods in terms of performance. Cho et al. [35] studied the dynamic behavior of hydrogen supply from an MH tank and its control of applications such as fuel cell systems. It was found that a proportional-integral-differential (PID) controller using recirculating water as heat exchanger fluid and temperature as the control variable was able to control the hydrogen supply. In a similar work, a mathematical model for dynamic discharge from MH hydrogen storage was developed by Aruna and Christa [36], and the performances of PID and Fuzzy-PID controllers were investigated. It was found that the performance of the Fuzzy-PID controller was slightly better than the conventional PID controller with lower

oscillations. Krane et al. [37] studied dynamic modeling and model predictive control of the two-reactor MH system. It was shown that the linearized model could accurately predict the behavior of the non-linear MH dynamics and that multivariate control is capable of its continuous operation. Keow et al. [38] developed a control-oriented model of MH hydrogen storage and studied the performance of active disturbance rejection control (ADRC) and proportional-integral (PI) controllers. It was found that both controllers could reduce the disturbances and maintaining the required hydrogen pressure in the tank; however, ADRC showed lower oscillations.

Based on the literature review, it can be noted that the coupled MH systems have great potential to provide renewable energy-based heating and cooling solutions. Nonetheless, temperature-driven MH heating and cooling systems are relatively less explored, especially for space conditioning applications in buildings. Additionally, while dynamic modeling of MH systems is commonly studied, their control-based investigations are scarcely investigated. The present work focuses on the control-based dynamic modeling of a temperature-driven coupled MH cooling system to regulate thermal demand in buildings. The main contributions, and novelties of this study can be outlined as follows.

- A simplified thermochemical dynamic model of the temperature-driven coupled MH cooling system is developed in the MATLAB® Simulink.
- A methodology is highlighted for selection and testing of potential higher-performing MH pairs in terms of COP values.
- A parametric investigation is performed to demonstrate the effects of operating temperatures on the system's performance.
- Finally, a PI control methodology is suggested for the dynamic control of the coupled MH cooling system with reference to the building cooling load.

## 3. Material and Methods

### 3.1 Selection of MH pairs

The selection of an MH pair is a crucial step in designing a temperature-driven MH-based heating and cooling system. For the proposed cooling application, a pair of MH is required to mutually transfer hydrogen during the charging and discharging cycles. Typically, one of the MHs needs to be of high operating temperature (HTMH) while another needs to be of low operating temperature (LTMH). In the first half of the cycle, termed the charging or regeneration cycle, the HTMH receives heat (e.g. waste heat or solar energy) and releases hydrogen that is being absorbed by the LTMH. In the second half of the cycle, termed the discharging or cooling cycle, LTMH produces a cooling effect by releasing hydrogen that is being absorbed by the HTMH. The cooling effect produced by the LTMH can be utilized to handle the thermal load of a building using appropriate heat exchange (HX) mechanisms. A schematic diagram of the HTMH and LTMH combined system is shown in Fig. 1.

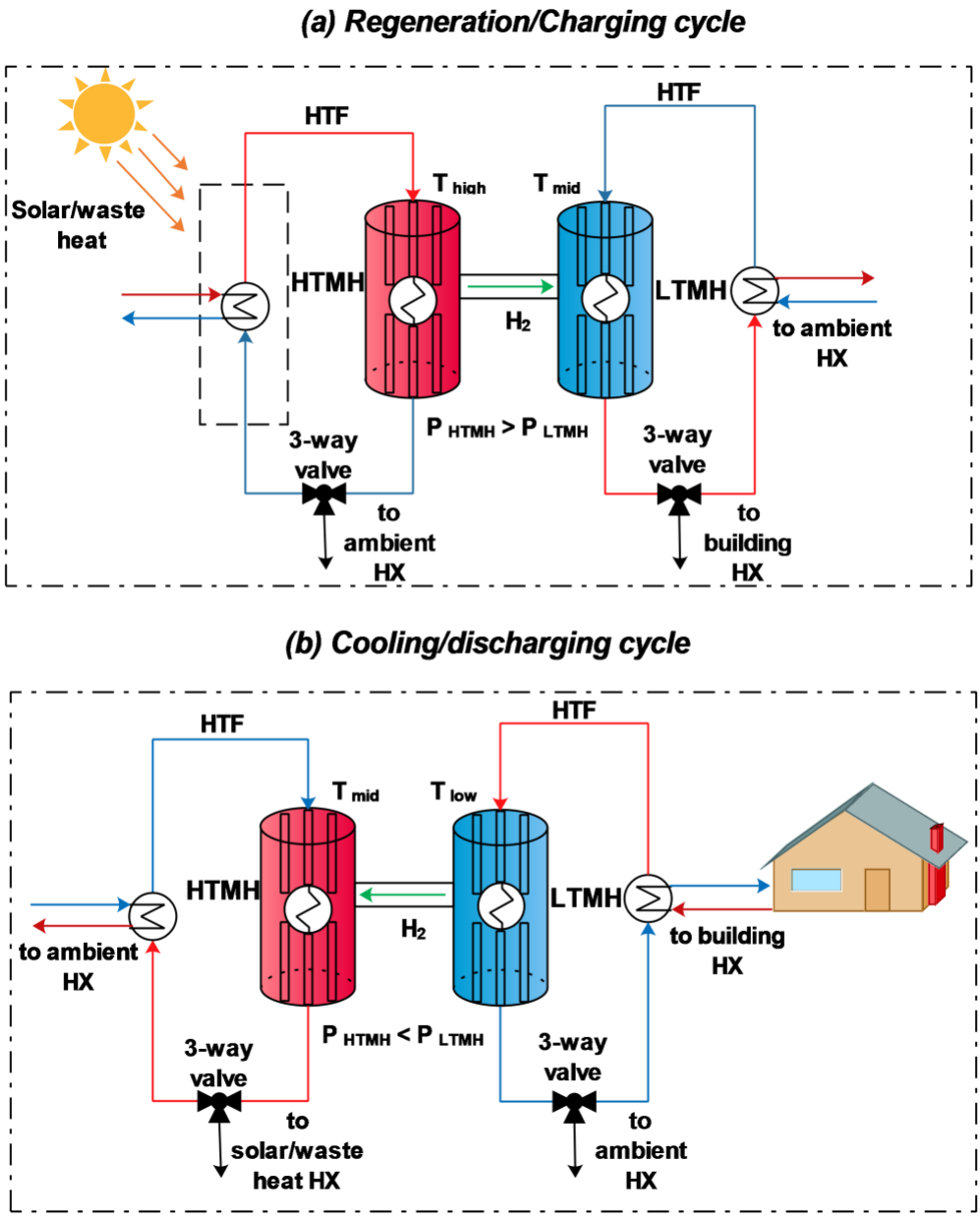


Fig. 1: Schematic of the temperature-driven coupled MH cooling system, (a) Regeneration or charging cycle, (b) Cooling or discharging cycle.

However, the transfer of hydrogen in the absence of an external power source can only be driven by the pressure difference between the two hydrides. It requires that the equilibrium pressures of the MHs are suitably matched for continuous operation under charging and discharging conditions. This criterion can be defined with the help of Van't Hoff equation, which results in the following conditions: [39]

Charging cycle: $P_{HTMH}(T_{high}) > P_{LTMH}(T_{mid})$ (1)

Discharging cycle: $P_{HTMH}(T_{mid}) < P_{LTMH}(T_{low})$ (2)

where $P_{HTMH}$ *and* $P_{LTMH}$ represent the equilibrium pressures of HTMH and LTMH, respectively at the charging and discharging conditions corresponding to the high operating temperature ($T_{high}$), mid operating temperature ($T_{mid}$), and low operating temperature ($T_{low}$).

A suitable high and low-temperature MH combination needs to be selected based on their pressure-temperature characteristics for the given operating conditions.

### 3.1.1 Methodology and selection criterion

The COP of the coupled MH system mainly depends on the capacity to exchange hydrogen between them, which is governed by their thermochemical properties. The equilibrium pressures at the given operating temperatures of the coupled MH system decides their capability to exchange hydrogen. Since equilibrium pressure varies with the hydriding and dehydriding of the MH, a parameter known as the hydriding efficiency is defined by Voskuilen et al. [40, 41] to estimate the equilibrium points for hydrogen transfers. A graphical representation of hydriding efficiency and corresponding Van't Hoff plot is shown in Fig. 2 for a hydride pair ($Zr_{0.76}Ti_{0.24}Ni_{1.16}Mn_{0.63}V_{0.14}Fe_{0.18}$, and $Ti_{0.85}Zr_{0.15}Cr_{1.2}Mn_{0.8}$) used in the present study. The MH concentration-pressure graph (Fig. 2. (a)) is used to obtain the equilibrium points for hydrogen transfers. In the graph, $x_{LTMH}$ and $x_{HTMH}$ denote the points at which hydrogen transfer will be stopped during charging and discharging cycles respectively due to pressure equilibrium. These equilibrium points in the concentration-pressure graph for hydrogen transfer are defined by:

$$x_{HTMH} = 1 - \frac{w_{HTMH}}{w_{HTMH,max}} \tag{3}$$

$$x_{LTMH} = \frac{w_{LTMH}}{w_{LTMH,max}} \tag{4}$$

The hydriding efficiency ($\eta_{hyd}$) of the system is then calculated by: [40,41]

$$\eta_{hyd} = (x_{LTMH} - x_{HTMH}) \tag{5}$$

While there are a large number of MH pair combinations theoretically possible, the MH MATLAB toolbox developed by Voskuilen et al. [42] is used in the present work to identify potential MH pairs in the proposed coupled MH-based cooling system. The toolbox incorporates a wide range of data for 337 metal hydrides gathered from approximately 150 literature sources. In addition to that, it also provides well-structured classifications such as MH types, thermophysical properties, kinetic parameters etc. Therefore, the toolbox enables a variety of analyses on different types of hydrides while respecting their individual characteristics. In the present work, this toolbox is used for the selection of MH pairs by evaluating their potential combinations in the coupled MH system as HTMH or LTMH. However, a data set of 337 metal hydrides generates a large number of possible pairs; the evaluation of all the possible MH pair combination is not only computationally intensive but also unrewarding as most of the pairs are bound to perform poorly. At this point, the idea of hydriding efficiency can effectively be introduced for selection of the MH pairs in the cooling system. In the present work, minimum 30% hydriding efficiency is chosen as the criteria for the MH pair selection. Furthermore, pressure boundary conditions are also need to be defined that are chosen as 1 bar to 150 bar as the minimum and maximum limits respectively. The minimum pressure limit is chosen to avoid a below atmospheric pressure conditions, whereas

the maximum pressure limit is chosen as a reasonable value considering the mechanical strength of the pressure vessels for designs of the HTMH at $T_{high}$ condition. A user-defined MATLAB function is developed, which incorporates the built-in thermodynamics pressure-composition-temperature (PCT) model to determine the intersection points of the isotherms and evaluate the maximum pressure, minimum pressure, and hydriding efficiency of a given hydride pair.

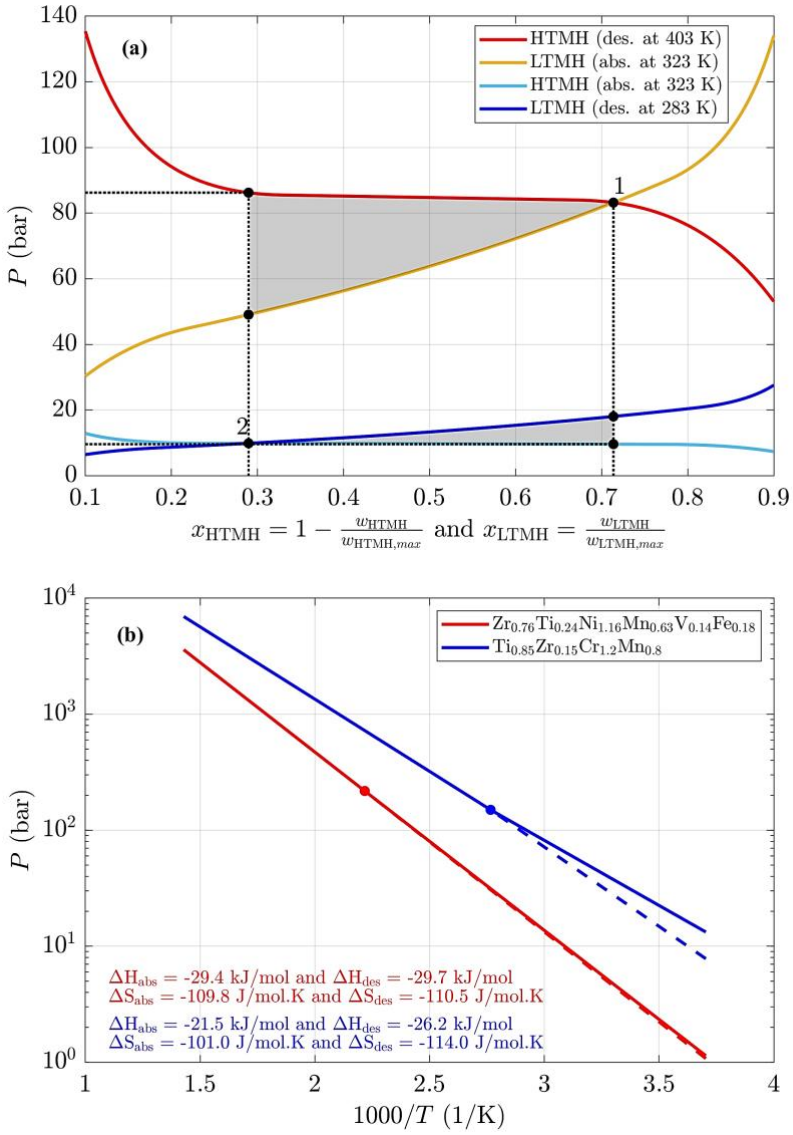


Fig. 2: Graphical representation of (a) hydriding efficiency, (b) Van't Hoff plot of a metal hydride pair selection.

In the present work, only the hydrides having single-plateau PCT models are considered. From the database of 337 hydrides, 325 hydrides have single-plateau PCT models. The combinations of these 325 hydrides are calculated, thus resulting in 105,300 unique hydride pairs. The MATLAB parallel processing functionality is used to run the code in an Intel Core i7-8550U processor. The selection criteria discussed earlier are then applied to all

these hydride pairs, and 1606 pairs are found to be suitable for use in the MH cooling system. A flow chart is shown in Fig. 3, illustrating the methodology of MH selection.

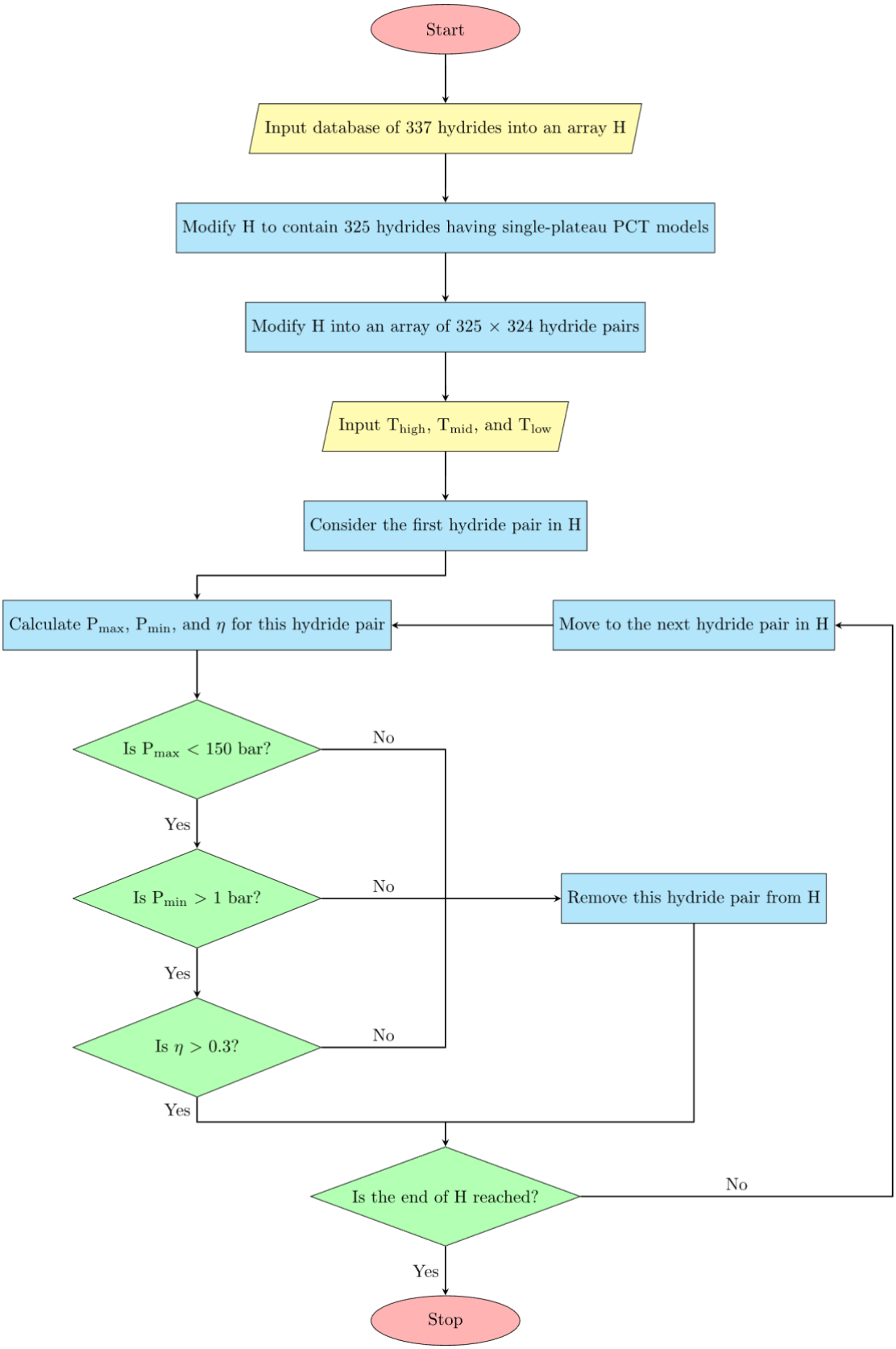


Fig. 3: Flow chart for the methodology of MH selection.

The following assumptions were made in this investigation:

- The MH reactor is assumed to be a lumped system with uniform temperature (in the direction of HTF); it only transfers heat to a heat transfer medium. MH reactor is assumed to be insulated from the outside, therefore heat loss to the ambient is neglected.
- The accuracy of model depends on the thermophysical properties of the MH reactors. Since, the temperature variation is relatively small in the present work, the thermophysical properties of the MH reactors are assumed independent of temperature in the given operating ranges.
- Heat transfer through the MH system is assumed to be dominated by conduction and convection; radiative heat loss is neglected. However, it could be applicable to high-temperature MH reactors such as Mg-based systems, where radiative heat loss is considerable.
- Hydrogen is assumed to follow ideal gas behavior, which is a reasonable assumption for the given operating conditions.
- It is assumed that there is a local thermal equilibrium between MH material and hydrogen. It allows for model simplification and reduced computational cost at minimal loss of accuracy.
- The building transient modeling is not considered for simplification. Instead, a representative building load is considered for the transient load response of an MH cooling system.
- The studied model estimates the theoretical transient response of the MH cooling system without considering losses to the balance of plants, such as heat exchangers, fans, pumps etc., to the building's thermal demand. Therefore, performance of the MH cooling system will be higher than the actual performance of a building cooling system.

### 3.2 Model description

A dynamic model of the coupled MH system is developed considering the thermophysical properties of the MH alloys, chemical kinetics, and equilibrium pressures, along with heat and mass transfer characteristics between the MH pairs. Therefore, each process can be described by a specific differential equation, necessitating a comprehensive dynamic model to predict the temporal changes of variables such as MH pressure, temperature, and hydrogen transfer rate between the hydrides. The detailed modeling approach is explained in appendix B.

### 3.3 Control Methodology

The primary objective of the control strategy used in this study is to meet the required cooling demand in the building. As shown in Fig. 4, three control loops are used to serve this purpose. Control loop 1 is used to control the flow rate of HTF to regulate the reference temperature of the MH reactors. The block diagram of control loop 1 is shown in Fig. 5(a). Control loop 2 is used for controlling the reference cooling load demand. A closed loop control is framed to control the temperature of the building to handle any disturbances in the control loop associated with the cooling demand. The block diagram of cooling loop 2 is shown in Fig. 5(b). The reference cooling load is calculated as per Eq. 9. The PI controller is used to generate the

control signal (hydrogen flow rate between two MH reactors) to maintain the required cooling demand. Control loop 3 is used to control the area (by modulating the $Cv$) of the hydrogen supply valve for regulating the required hydrogen flow between the MH reactors. The output (hydrogen supply-demand) of control loop 2 provides the reference signal for control loop 3, while the actual hydrogen supply between the MH reactors is estimated using Eq. B.6. The difference between the reference and actual output is used as input for the PI control. The proportional term generates the control signal corresponding to the difference between the reference and actual outputs, while integral time benefits by minimizing the steady-state error. Tuning of the PI (selection of the proportional $K_p$ and integral $K_i$) is essential for the stability and output response of the overall control system. In this study, tuning of the PI parameters is performed using the Ziegler-Nicolas method [43]. The values of $K_p$ are 0.9 and 0.498, and of $K_i$ are 0.0001 and 0.0001 for control loops 1 and 2, respectively.

The relationship between the input and output for the control loop 1 can be expressed as given below:

$$\frac{T}{T_{ref}} = \frac{G_{PI,1}G_{0,1}}{1+G_{PI,1}G_{0,1}} \tag{6}$$

The input-output relation for control loop 2 can be provided as below:

$$\frac{\dot{Q}_L}{(\dot{Q}_L)_{ref}} = \frac{G_{PI,2}G_{0,2}}{1+G_{PI,2}G_{0,2}} \tag{7}$$

The transfer function for the control loop 3 can be formulated as given below:

$$\frac{\dot{m_{H_2}}}{(\dot{m_{H_2}})_{ref}} = \frac{G_{PI,3}G_{0,3}}{1+G_{PI,3}G_{0,3}} \tag{8}$$

where $G_{PI,i}$ is the PI control loop, $G_{0,i}$ is the plant equation, and $i$ = 1,2,3 for loops 1, 2, and 3. $\dot{Q}_L$ is the cooling load while $\dot{m_{H_2}}$ is the hydrogen flow rate between the hydride tanks. $T$ is temperature, and *ref* denote the reference values.

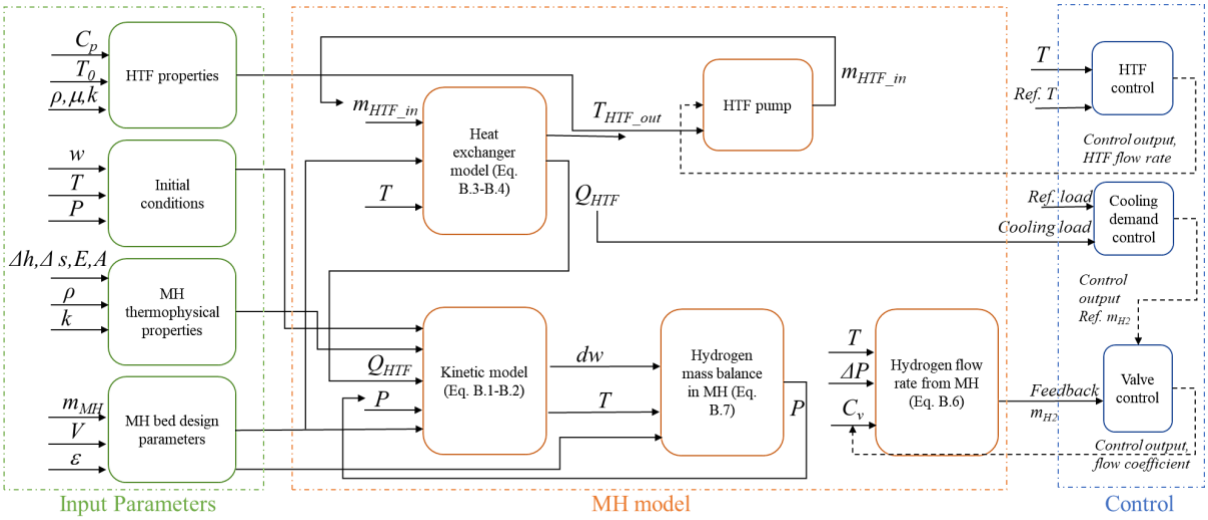

Fig. 4: Block diagram of the modeling and control methodology.

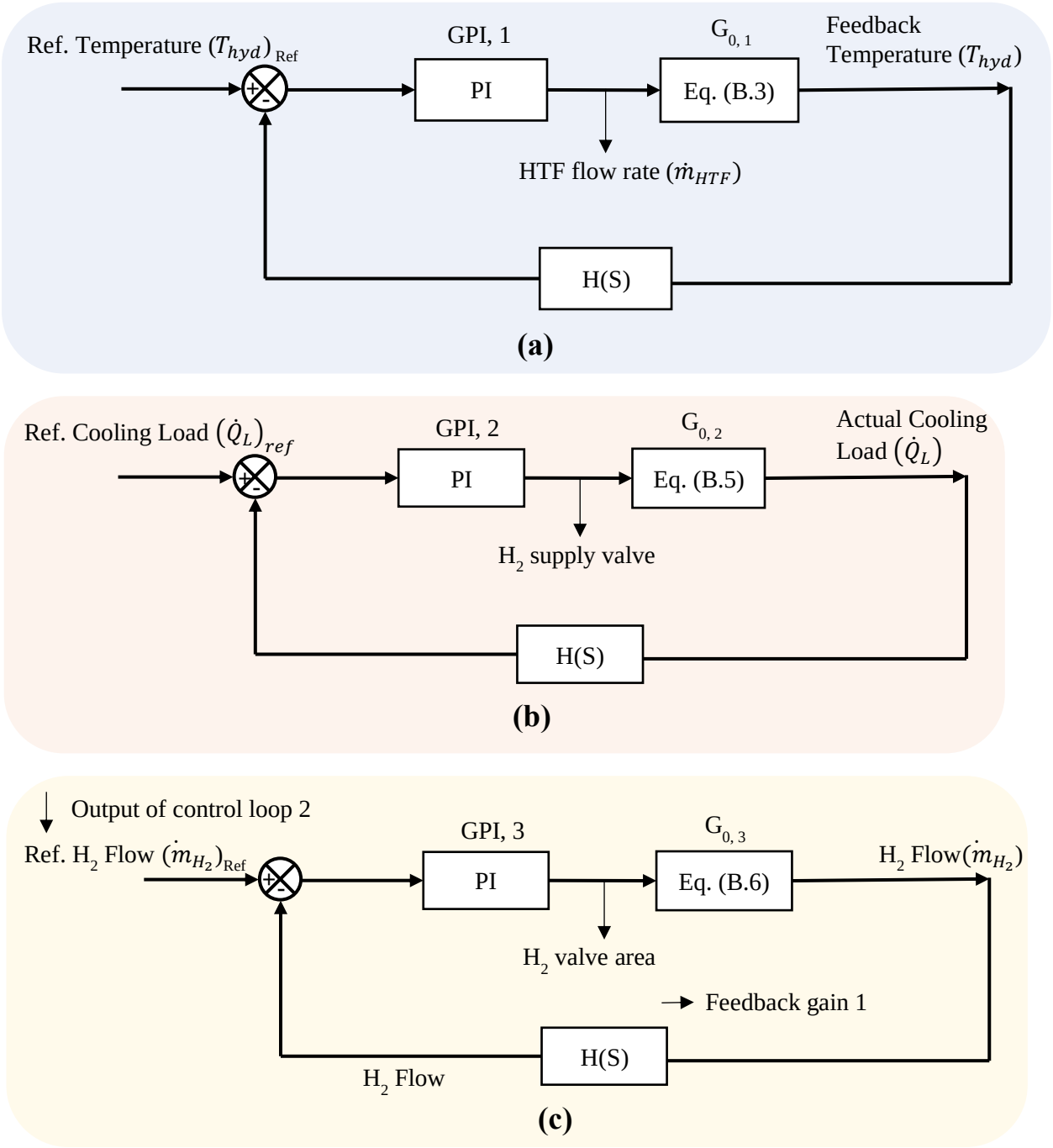


Fig. 5: Block diagram of the control methodologies, (a) control loop 1 to regulate flow rate of HTF, (b) control loop 2 to regulate cooling load demand, (c) control loop 3 to regulate hydrogen flow rate between MHs.

The time-varying cooling load profiles are used to study the transient operational performance of the coupled MH system. First, a standard step signal-based representative cooling load demand is used to study the control response of the developed system. Thereafter, an actual outdoor condition (location – New Delhi 28.6341° N, 77.2169° E, on a sunny day) based on cooling load demand for a building is used for the analysis. The cooling load demand is mainly dependent on the heat loss to the environment, internal heat gain, and solar heat gain,

which varies with time. Therefore, a simple methodology is adopted to calculate the building cooling load that depends on the ambient temperature and the solar irradiation. [10]

$$\left(\dot{Q}_L\right)_{ref} = (U.A)_b.(T_{amb} - T_{set}) + \dot{Q}_{IHG} + \dot{Q}_{SHG} \quad (9)$$

where $U_b$, and $A_b$ represent the overall heat transfer coefficient and available area of heat transfer for the cooling space, respectively. A typical single-story office building [44] with a floor area of about 490 $m^2$ has been considered for reference load calculation. It has an average overall heat transfer coefficient of 4 $W/m^2$ K and an envelope surface area of 600 $m^2$ for heat transfer. $T_{set}$ shows the desired indoor set point temperature, which is taken as 25°C. $\dot{Q}_{IHG}$ is the internal heat gain, which is considered constant at 26 kW. $\dot{Q}_{SHG}$ is the heat gain due to solar radiation, which is proportional to the global horizontal irradiation (GHI) as follows:

$$\dot{Q}_{SHG} = \frac{GHI}{GHI_{max}}.\left(\dot{Q}_{SHG}\right)_{max} \quad (10)$$

where $\left(\dot{Q}_{SHG}\right)_{max}$ is taken as 500 $W/m^2$ in the present work [44]. The studied building needs a peak cooling demand of 227.14 kW. However, for ease of calculation and the reader's understanding, the coupled MH system is designed for a peak cooling demand of 1 kW. Therefore, the cooling load profile is normalized accordingly for the present analysis.

### 3.4 Performance parameters

The operating temperatures of the coupled MH system, which are $T_{high}$, $T_{low}$, $T_{mid}$, and $T_{amb}$ have the most significant influence on the overall system performance. Hence, the effects of these temperatures are studied, and various trends in the system behavior are identified.

The COP of this system is given by the ratio of the total heat transferred to the LTMH and HTMH: [45]

$$COP = \frac{Q_L}{Q_H} \quad (11)$$

where $Q_L$ is the cooling output in the cooling cycle, and $Q_H$ is the heat input in the regeneration cycle. In addition to the COP, another important performance parameter is the second law efficiency ($\eta$), which is defined as the ratio of the COP of the actual cooling system to that of an idealized or reversible cooling system under the same operating conditions. The second law of efficiency for a temperature-driven MH cooling system is given by the following expression: [45]

$$\eta = \frac{COP}{COP_{rev}} = COP\,\frac{\left(\frac{T_{mid}}{T_{low}} - 1\right)}{\left(1 - \frac{T_{mid}}{T_{high}}\right)} \quad (12)$$

The other parameters used in the present analysis are specific heating power (SHP) and specific cooling power (SCP), denoted by $\dot{q}_H$ and $\dot{q}_L$, respectively, which are helpful for the practical design of MH thermal systems. This is because they provide direct information on the hydride masses required for a particular heating or cooling load [30].

$$\dot{q}_H = \frac{Q_H}{\tau_1(m_{HTMH}+m_{LTMH})} \quad (13)$$

$$\dot{q}_L = \frac{Q_L}{\tau_2(m_{HTMH}+m_{LTMH})} \quad (14)$$

where $m_{HTMH}$ and $m_{LTMH}$ are the masses of hydrides HTMH and LTMH, respectively. $\tau_1$ and $\tau_2$ are the cycle times for the charging and discharging half cycles, respectively. The importance of SHP and SCP compared to COP and second law efficiency depends on the end applications. For example, in a portable system, the weight would be given more importance compared to a stationary system

### 3.5 Solution method

Fig. 1 depicts the schematic of two half-cycles of a temperature-driven MH cooling system. Each of them consists of a pair of MH reactors (HTMH and LTMH) that exchange hydrogen between them by absorbing and rejecting heat from the source and sink respectively. Based on the methodology discussed in the previous sections, a thermochemical model is prepared in a MATLAB Simulink environment to simulate the dynamic behavior of a temperature-driven MH cooling system. The dynamics of this system such as reaction kinetics, change in hydride reactor temperature, pressure, and mass of hydrogen are given by ordinary differential equations (ODEs). The ode23tb (stiff/TR-BDF2) is a variable-step solver that is used in the present Simulink model, and the system of ODEs is solved for the two half-cycles. The system performance is studied at 130°C, 50°C, and 10°C as $T_{high}$, $T_{mid}$, and $T_{low}$, respectively. The ambient temperature $T_{amb}$ of 30°C is assumed. The MH cooling system conditions used in this analysis are listed in Table 1. The hydride reactor porosity is considered 30% for both the reactors as a conservative value. The maximum and minimum hydrogen mass fractions are selected to increase the MH operation in the plateau region. The operating temperature ranges are selected considering a building application, and environmental constraints. Different heat transfer fluids (HTF) are considered for HTMH and LTMH depending on their operating temperature limits.

Table 1: Initial conditions and the input parameters used in the present analysis.

| Parameter | HTMH | LTMH |
|---|---|---|
| Hydride reactor porosity | 30% | 30% |
| Initial temperature | 30°C | 30°C |
| Maximum hydrogen mass fraction | 0.9 | 0.9 |
| Minimum hydrogen mass fraction | 0.1 | 0.1 |
| Operating temperatures | 130°C and 50°C | 50°C and 10°C |
| Solver type | Variable-step solver | Variable-step solver |

| | | |
|---|---|---|
| The initial temperature of HTF | 30°C* | 30°C* |
| Heat transfer fluid (HTF) | Paratherm oil | 50% (v/v) Ethylene glycol/water |

* Variable HTF temperature is considered with dynamic load operations under building load.

### 3.6 Model validation

As a good practice, any computational model is validated with the available literature to ensure accuracy. The present model is validated with the heat pump system discussed in [40] under the identical operating conditions. The COP values of a few selected hydride combinations are compared between the two models, as shown in Table 2. These values are found to be in close agreement with each other, thus validating the model.

Table 2: Comparison of the COP of heat pump system for the present analysis with the available literature.

| **HTMH** | **LTMH** | **COP** | |
|---|---|---|---|
| | | **Waters et al. [40]** | **Present model** |
| $V_{0.8455}Ti_{0.1045}Fe_{0.05}$ | $MmNi_{4.6}Fe_{0.4}$ | 1.45 | 1.42 |
| $La_{0.65}Ce_{0.28}Pr_{0.07}Co_5$ | $V_{0.95}Cr_{0.05}$ | 1.44 | 1.48 |
| NaAl | $Ti_{0.8}Zr_{0.2}Mn_{1.5}Cr_{0.5}$ | 1.40 | 1.38 |
| $V_{0.8455}Ti_{0.1045}Fe_{0.05}$ | $Ti_{1.2}Cr_{1.2}Mn_{0.8}$ | 1.36 | 1.36 |
| $LaNi_5$ | $ErNi_3$ | 1.35 | 1.34 |
| $V_{0.8455}Ti_{0.1045}Fe_{0.05}$ | $Ti_{1.2}CrMn$ | 1.34 | 1.35 |
| $Y_2Co_7$ | $Er_2Co_7$ | 1.34 | 1.36 |
| $V_{0.8455}Ti_{0.1045}Fe_{0.05}$ | $Ti_{1.1}Cr_{1.2}Mn_{0.8}$ | 1.32 | 1.34 |

## 4. Results and discussion

### 4.1 Effect of MH pair selection

Based on the selection criteria discussed in section 3.1.1, 1606 hydride pairs were found to qualify for use in the coupled MH cooling system. Fig. 6 illustrates the 3D graph of 1606 MH pairs for each combination of HTMH and LTMH types. It can be seen that AB, $AB_2$, and $AB_5$, are most suitable MH types for the HTMH. Whereas, AB, $AB_2$, $AB_5$, and SS were found to be suitable MH types for the LTMH. It can also be noted from Fig. 6 that $AB_5$–$AB_2$ and $AB_5$–$AB_5$ MH pair formed most number of possible combinations among the qualified hydrides for

the coupled MH cooling system. One of the reasons for this result is due to the dominance of these MH types in the MATLAB toolbox database. Nevertheless, it also represents that these hydride pairs are most suitable for MH-based cooling systems, and they have been widely studied in the literature [46, 47].

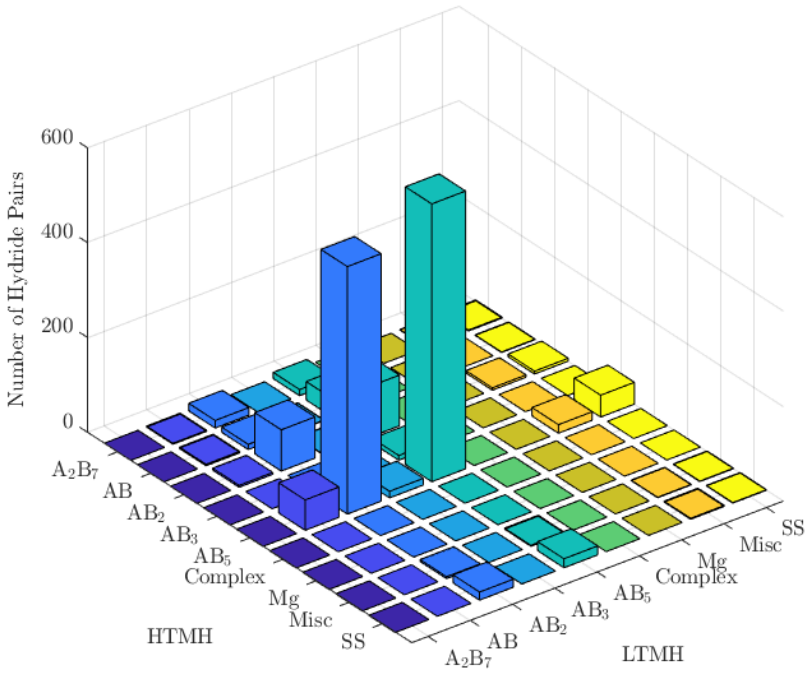


Fig. 6: A 3D graph of selected MH pairs for each combination of hydride types.

All these 1606 hydride pairs were studied in the coupled MH cooling model, and various performance parameters were recorded for the analysis. Initially, the COP values of all the hydride pairs were calculated to identify the most promising pair, which is the ratio of total heat transferred to the LTMH and HTMH as given by Eq. (11). The distribution of the resulting COP values is plotted in Fig. 7 for all the hydride pairs. It can be observed that a large number of hydride pairs have COP values between 0.4 and 0.6, but this number decreases gradually for higher COP values. Furthermore, the COP values were found to be sensitive to the range of operating temperatures. The results presented are obtained for temperatures of 130°C, 50°C, and 10°C for the high, middle, and low temperatures, respectively. It was found that more hydride pairs with higher COP values can be obtained by lowering the middle temperature. It can also be noted that the kinetics of some hydrides vary considerably over charging and discharging cycles, which require changes in the model and may affect the system results. Table 3 lists the top 20 MH pairs showing the highest COP values out of the 1606 hydride pairs studied in this work. It can be seen that although top MH pairs have high COP values, their cycle times are very large. A large cycle time would make the cooling system impractical due to its poor utilization. However, the MH pair $Zr_{0.76}Ti_{0.24}Ni_{1.16}Mn_{0.63}V_{0.14}Fe_{0.18}$–$Ti_{0.85}Zr_{0.15}Cr_{1.2}Mn_{0.8}$ shows comparatively fast reaction kinetics with regeneration cycle time of 2.45 hours and cooling cycle time of 7.5 hours under the given operating conditions. Also,

the hydride pair $Zr_{0.76}Ti_{0.24}Ni_{1.16}Mn_{0.63}V_{0.14}Fe_{0.18}$ and $Ti_{0.85}Zr_{0.15}Cr_{1.2}Mn_{0.8}$ produced a high COP value of 0.71 as shown in Table 3. The heat transferred to the MH reactors depends on the changes in enthalpy ($\Delta H$) and hydrogen mass exchange during desorption process. Therefore, a coupled MH cooling system should have low changes in enthalpy for HTMH and high changes in enthalpy for LTMH during desorption process (see Table 4). As COP of the coupled MH cooling systems is the ratio of total heat transferred to the LTMH and HTMH, such a system offers higher COP. Furthermore, a high maximum hydrogen mass fraction capacity of hydride allows for more amount of hydrogen exchange during the half cycle, which results in increased total heat transfer. The other thermophysical properties such as density, porosity and thermal conductivity of the MH reactor can also affect the total heat transfer, and consequently the COP. Therefore, the hydride pair $Zr_{0.76}Ti_{0.24}Ni_{1.16}Mn_{0.63}V_{0.14}Fe_{0.18}$, and $Ti_{0.85}Zr_{0.15}Cr_{1.2}Mn_{0.8}$ was chosen for the further parametric study. It can be noted that in a practical MH-based thermal system, the MH selection can be based on many more criteria, such as high thermal conductivity, fast reaction kinetics, large hydrogen storage capacity, stable thermophysical properties, chemical reversibility, and low cost, etc. [47]. In the present work, the initial selection criterion and system COP consider some of these features but not all of them. However, COP can be employed as the decision-making tool along with the remaining criteria and is helpful for such analysis. The hydride pair ($Zr_{0.76}Ti_{0.24}Ni_{1.16}Mn_{0.63}V_{0.14}Fe_{0.18}$, and $Ti_{0.85}Zr_{0.15}Cr_{1.2}Mn_{0.8}$) is an $AB_2$- $AB_2$ type MH pair, which is considered to have fast reaction kinetics in the literature [27, 48]. Nevertheless, the subsequent parametric analysis and control system results are expected to have a generalized behavior with the other hydride pairs as well.

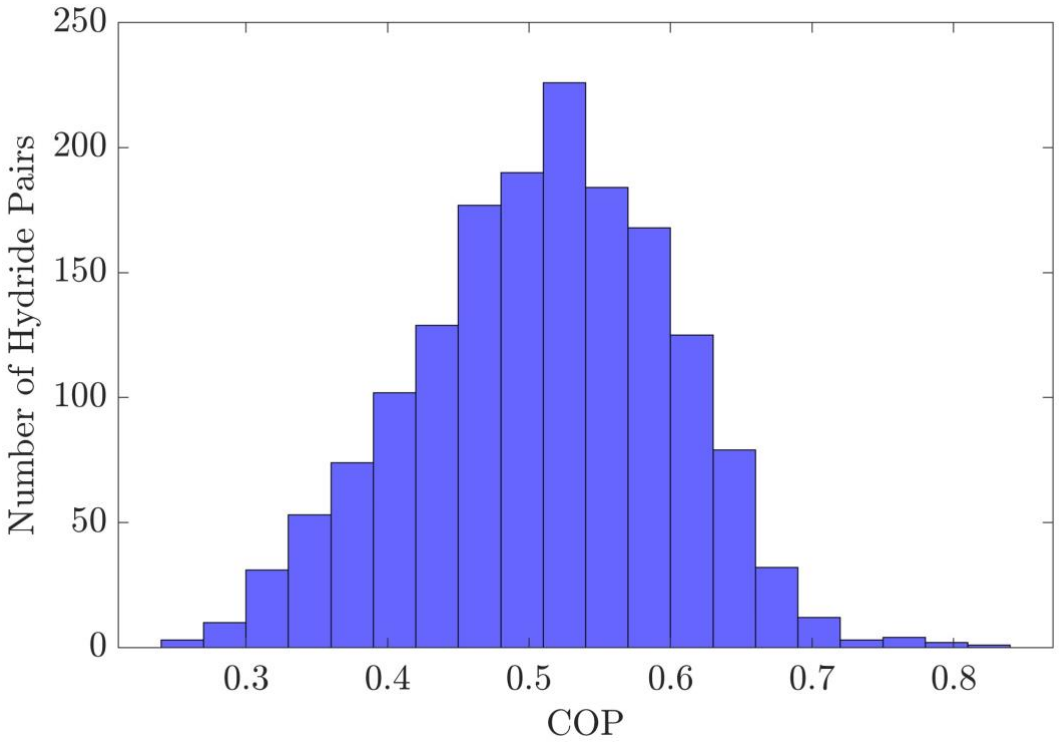


Fig. 7: COP distribution for all suitable MH pairs in a coupled MH-based cooling system.

Table 3: COP and cycle time of the top 20 hydride pairs for coupled MH cooling system based on the present analysis.

| HTMH | Cycle time, $\tau_1$ (hour) | LTMH | Cycle time, $\tau_2$ (hour) | COP |
|---|---|---|---|---|
| $Zr_{0.76}Ti_{0.24}Ni_{1.16}Mn_{0.63}V_{0.14}Fe_{0.18}$ | 4.88 | $MmNi_{4.6}Fe_{0.4}$ | 15.43 | 0.82 |
| $LaNi_{4.7}Al_{0.3}$ | 26.55 | $Zr_{0.76}Ti_{0.24}Ni_{1.16}Mn_{0.63}V_{0.14}Fe_{0.18}$ | 45.74 | 0.80 |
| $LaNi_{4.65}Mn_{0.2}Al_{0.15}$ | 8.44 | $MmNi_4Cu_{0.7}Ti_{0.1}Sn_{0.1}Fe_{0.1}$ | 56.94 | 0.79 |
| $LaNi_5$ | 9.88 | $Mm_{0.9}Ti_{0.1}Ni_5$ | 27.83 | 0.77 |
| $LaNi_{4.75}Sn_{0.25}$ | 17.71 | $Mm_{0.5}Ca_{0.5}Ni_{2.5}Co_{2.5}$ | 72.54 | 0.77 |
| $LaNi_{4.8}Sn_{0.2}$ | 19.78 | $MmNi_3Co_2$ | 69.03 | 0.75 |
| $CaNi_5$ | 42.45 | $Zr_{0.76}Ti_{0.24}Ni_{1.16}Mn_{0.63}V_{0.14}Fe_{0.18}$ | 71.50 | 0.75 |
| $Zr_{0.76}Ti_{0.24}Ni_{1.16}Mn_{0.63}V_{0.14}Fe_{0.18}$ | 5.24 | $La_{0.4}Pr_{0.6}Co_5$ | 16.78 | 0.74 |
| $LaNi_{4.75}Sn_{0.25}$ | 47.13 | $MmNi_3Co_2$ | 50.38 | 0.73 |
| $Ti_{0.56}V_{0.3}Zr_{0.1}Mn_{0.94}Fe_{0.06}Ni_{0.04}$ | 1.95 | $Ti_{1.3}Cr_{1.2}Mn_{0.8}$ | 16.03 | 0.73 |
| $TiFe_{0.85}Ni_{0.15}$ | 6.97 | $MmNi_3Co_2$ | 66.54 | 0.72 |
| $LaNi_{4.7}Sn_{0.3}$ | 31.17 | $MmNi_3Co_2$ | 55.12 | 0.71 |
| $YNi_4Al$ | 100.59 | $MmNi_4Cu_{0.7}Ti_{0.1}Sn_{0.1}V_{0.1}$ | 27.73 | 0.71 |
| $ZrCrFe_{1.2}$ | 30.94 | $Zr_{0.76}Ti_{0.24}Ni_{1.16}Mn_{0.63}V_{0.14}Fe_{0.18}$ | 41.39 | 0.71 |
| **$Zr_{0.76}Ti_{0.24}Ni_{1.16}Mn_{0.63}V_{0.14}Fe_{0.18}$** | **2.45** | **$Ti_{0.85}Zr_{0.15}Cr_{1.2}Mn_{0.8}$** | **7.50** | **0.71** |
| $LaNi_{4.75}Sn_{0.25}$ | 7.77 | $LmNi_{4.91}Sn_{0.15}$ | 88.87 | 0.71 |
| $Ti_{0.8}Zr_{0.2}Mn_{1.5}V_{0.5}$ | 12.62 | $MmNi_4Cu_{0.7}Ti_{0.1}Sn_{0.1}Fe_{0.1}$ | 22.12 | 0.71 |
| $Ti_{0.8}Zr_{0.2}Mn_{1.5}V_{0.5}$ | 4.83 | $MmNi_4Cu_{0.7}Ti_{0.1}Sn_{0.1}V_{0.1}$ | 30.50 | 0.70 |
| $Zr_{0.76}Ti_{0.24}Ni_{1.16}Mn_{0.63}V_{0.14}Fe_{0.18}$ | 13.97 | $DyNi_{4.5}Al_{0.5}$ | 9.23 | 0.70 |
| $Zr_{0.9}Ti_{0.1}Cr_{0.9}Fe_{1.1}$ | 82.15 | $Zr_{0.76}Ti_{0.24}Ni_{1.16}Mn_{0.63}V_{0.14}Fe_{0.18}$ | 39.28 | 0.7 |

### 4.2 Effect of operating temperatures

Fig. 8 depicts the Van't Hoff diagram for the hydride pair of $Zr_{0.76}Ti_{0.24}Ni_{1.16}Mn_{0.63}V_{0.14}Fe_{0.18}$, and $Ti_{0.85}Zr_{0.15}Cr_{1.2}Mn_{0.8}$ showing the relationship of equilibrium pressure and temperature. The HTMH receives heat at $T_{high}$ represented by point 'A', thereby starting the desorption of hydrogen. Since the equilibrium pressure of LTMH (at point 'B') operating at $T_{mid}$ is lower than the equilibrium pressure of HTMH, desorbed hydrogen from HTMT is absorbed by

LTMH at point 'B'. The process of hydrogen transfer from points A to B is represented as the regeneration cycle. Thereafter, the LTMH and HTMH are cooled down to temperatures $T_{low}$ and $T_{mid}$, respectively, as represented by points 'C' and 'D'. It can be seen that the equilibrium pressure of LTMH is higher than the equilibrium pressure of HTMH at these operating temperatures. Therefore, LTMH receives heat at point 'C' (cooling effect) undergoing hydrogen desorption, and HTMH rejects heat at point 'D' undergoing hydrogen absorption. The process of hydrogen transfer from points 'C' to 'D' represents the cooling cycle. It is evident that the regeneration and cooling cycles are dependent on the operating temperatures that govern the performance of the coupled MH system. Therefore, a parametric investigation is performed in this section to understand the effect of temperature operating conditions on the performance of the coupled MH-based cooling system. The kinetic and thermodynamic parameters used in the simulation for the MH pair (HTMH - $Zr_{0.76}Ti_{0.24}Ni_{1.16}Mn_{0.63}V_{0.14}Fe_{0.18}$ and LTMH - $Ti_{0.85}Zr_{0.15}Cr_{1.2}Mn_{0.8}$) are shown in Table 4 and Table 5 respectively.

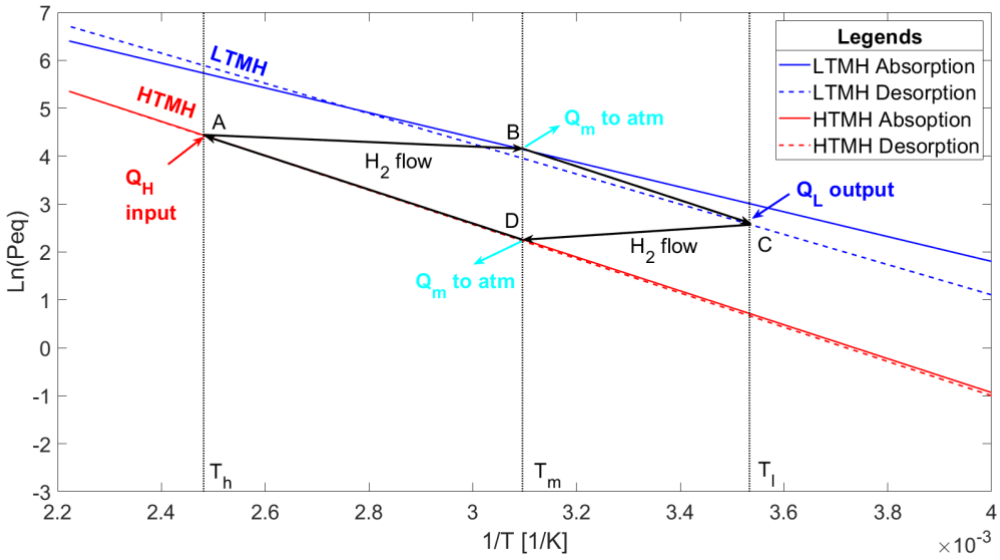


Fig. 8: Van't Hoff diagram showing the relationship of equilibrium pressure and temperature for the hydride pair of $Zr_{0.76}Ti_{0.24}Ni_{1.16}Mn_{0.63}V_{0.14}Fe_{0.18}$, and $Ti_{0.85}Zr_{0.15}Cr_{1.2}Mn_{0.8}$.

Table 4: List of kinetic parameters used in the simulation for HTMH - $Zr_{0.76}Ti_{0.24}Ni_{1.16}Mn_{0.63}V_{0.14}Fe_{0.18}$ and LTMH - $Ti_{0.85}Zr_{0.15}Cr_{1.2}Mn_{0.8}$ based coupled MH cooling system.

| **Parameter** | **Value** | | | |
|---|---|---|---|---|
| | **HTMH** | | **LTMH** | |
| | **Absorption** | **Desorption** | **Absorption** | **Desorption** |
| Arrhenius rate ($A$, 1/s) | 473 | 58 | 473 | 58 |

| | | | | |
|---|---|---|---|---|
| Activation energy ($E$, J/mol) | 24900 | 22100 | 24900 | 22100 |
| Order of reaction ($n$) | 1 | 1 | 1 | 1 |
| Material weight capacity ($w_{max}$) (kg $H_2$/kg MH material) | 0.01759 | 0.01759 | 0.020512 | 0.020512 |
| Changes in enthalpy ($\Delta H$, J/mol $H_2$) | -29393 | -29700 | -21500 | -26200 |
| Changes in entropy ($\Delta S$, J/mol.K) | -109.82 | -110.5 | -101.0 | -114.0 |

Table 5: List of thermodynamic parameters used in the simulation for HTMH - $Zr_{0.76}Ti_{0.24}Ni_{1.16}Mn_{0.63}V_{0.14}Fe_{0.18}$ and LTMH - $Ti_{0.85}Zr_{0.15}Cr_{1.2}Mn_{0.8}$ based coupled MH cooling system.

| **Parameter** | **Value** | |
|---|---|---|
| | **HTMH** | **LTMH** |
| Specific heat ($C_p$, J/kg.K) | 419 | 419 |
| Mass of MH ($m_{hyd}$, kg) | 284.25 | 243.76 |
| Void fraction | 0.3 | 0.3 |
| Material crystal density ($\rho$, kg/m$^3$) | 6700 | 6700 |
| Material thermal conductivity ($k$, W/m.K) | 1.6 | 1.6 |

Figures 9, 10, 11, and 12 show the variation of the performance parameters such as coefficient of performance (COP), second law efficiency ($\eta$), total heat transfers ($Q_H$ and $Q_L$), specific powers ($\dot{q}_H$ and $\dot{q}_L$), and cycle time ($\tau_1$ *and* $\tau_2$) with $T_{high}$, $T_{low}$, $T_{mid}$, and $T_{amb}$, respectively. Fig. 9 shows the effect of high temperature, $T_{high}$ at which HTMH is operated during the regeneration cycle. $T_{high}$ is varied between 120°C and 180°C while the other operating parameters are kept constant. In the regeneration cycle, an increase in $T_{high}$ causes increase in the equilibrium pressure of HTMH. As the $T_{mid}$ temperature is kept constant, it leads to an increased pressure gradient between HTMH and LTMH, which raises the driving potential of hydrogen transfer from HTMH to LTMH. The dehydriding of HTMH occurs at a faster rate, thus causing regeneration cycle time ($\tau_1$) to decrease as shown in Fig. 9(c). Since the total amount of hydrogen transferred from HTMH to LTMH remains nearly constant, the variation in MH reaction heat is also small. However, the total heat transferred, $Q_H$ to HTMH, increases with $T_{high}$ due to sensible heating of the HTMH to higher temperatures as shown in Fig. 9(b). The cooling load, $Q_L$ remains constant, as it does not depend on $T_{high}$. Therefore, the

COP of the system decreases almost linearly with $T_{high}$ as shown in Fig. 9(a). However, the second law efficiency decreases as the $T_{high}$ increases because of the increased availability of the heat input at higher values of $T_{high}$. It can be understood that for extracting the same quantity of low-grade heat energy ($Q_L$), higher quality of heat energy $Q_H$ is used with higher $T_{high}$ values. For example, the reversible COP$_{rev}$ values with $T_{high}$ of 140°C and 180°C are 1.54 and 2.03, respectively, however, actual COP values remain constant. Nevertheless, higher values of $T_{high}$ lead to shorter cycle time and hence increase the specific heating power, $\dot{q}_H$. A shorter cycle time and higher heating power would be useful for compact and fast-responding thermal systems.

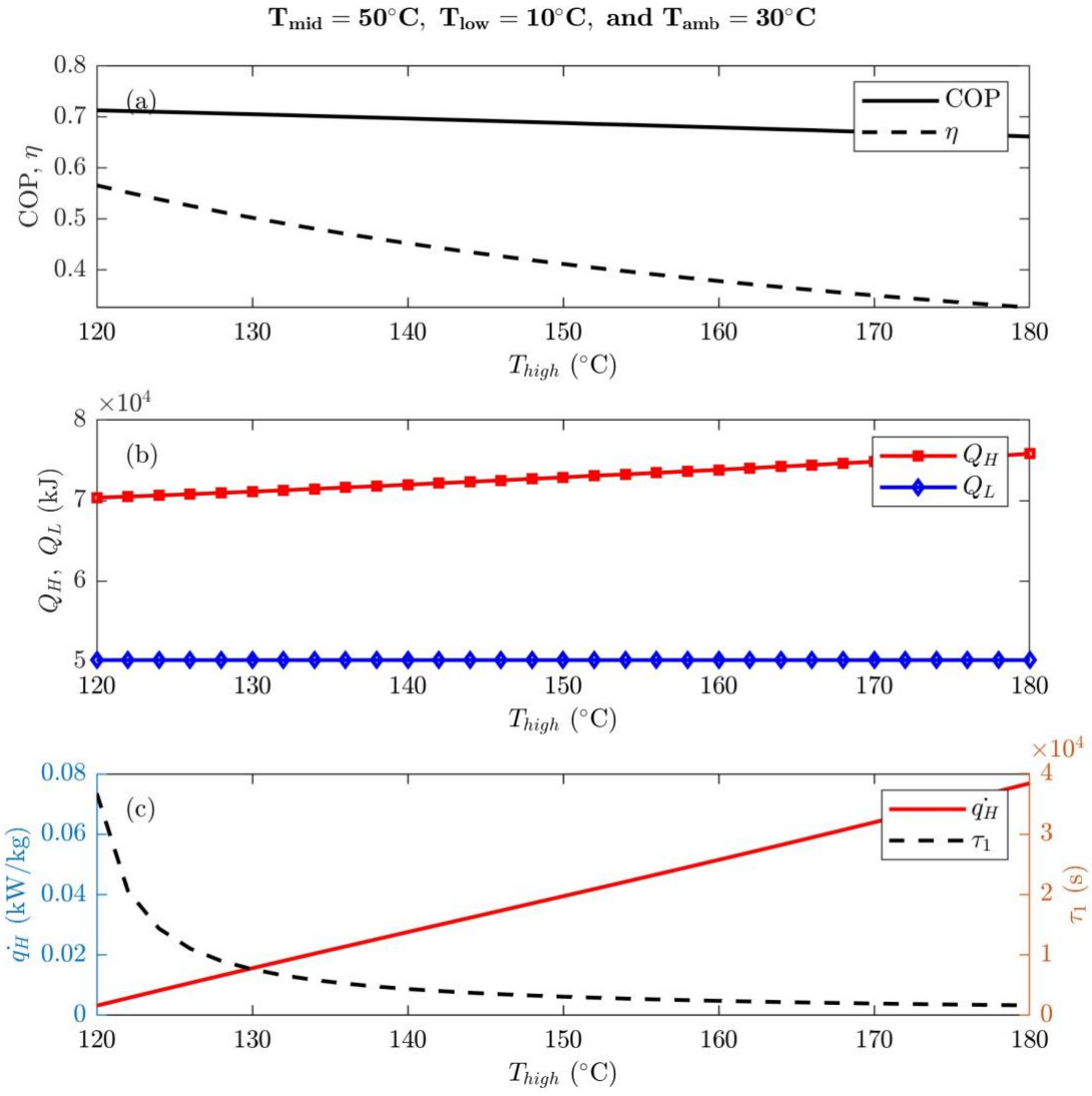


Fig. 9: Effect of high-temperature, $T_{high}$ for HTMH during the regeneration cycle.

The cooling effect is produced by LTMH during the second half of the cycle (cooling/discharge cycle); the effect of low temperature, $T_{low}$, at which LTMH is operated during the cooling cycle, is shown in Fig. 10. $T_{low}$ is varied between 0°C to 25°C keeping other operating parameters constants. It is found that at $T_{low}$ near 0°C, the equilibrium pressures of

LTMH and HTMH are very close resulting in poor mass transfer between the hydrides. It is reflected in the low total heat transfer from LTMH, $Q_L$ as shown in Fig. 10(b). An increase in $T_{low}$ causes increase in the equilibrium pressure of the LTMH. As $T_{mid}$ is kept constant, it results in an increased pressure gradient between the LTMH and HTMH, which raises the driving potential of hydrogen transfer from LTMH to HTMH. It is reflected as the increased heat transfer from the LTMH, which is an increase in the cooling effect. Therefore, the COP of the coupled MH cooling system increases with the increase in $T_{low}$ as shown in Fig. 10(a). However, COP values do not vary significantly after 10°C as total hydrogen transfer capacity approaches saturation and changes marginally afterwards. Although COP increases, the second law efficiency decreases as $T_{low}$ increases because of the reduced availability of the cooling output at higher values of $T_{low}$ as shown in Fig. 10(a). That is because $COP_{rev}$ increases with higher values of $T_{low}$, however, actual COP does not increase in the same manner. Fig. 10(b) shows that the total heat transferred, $Q_L$ to LTMH changes marginally with $T_{low}$ at higher temperatures. The heating load, $Q_H$ remains constant, as it does not depend on $T_{low}$. On the other hand, dehydriding of the LTMH occurs at a faster rate with higher $T_{low}$ values, thus causing $Q_L$ to increase and cooling cycle time $\tau_2$ to decrease. This results in a gradual increase in specific cooling power $\dot{q}_L$ as shown in Fig. 10(c). It can be noted that the low $\dot{q}_L$ values of the MH system are due to the restricted flow rate of the hydrogen in the present design. It can be further increased by regulating the hydrogen flow rate, as shown in the next section.

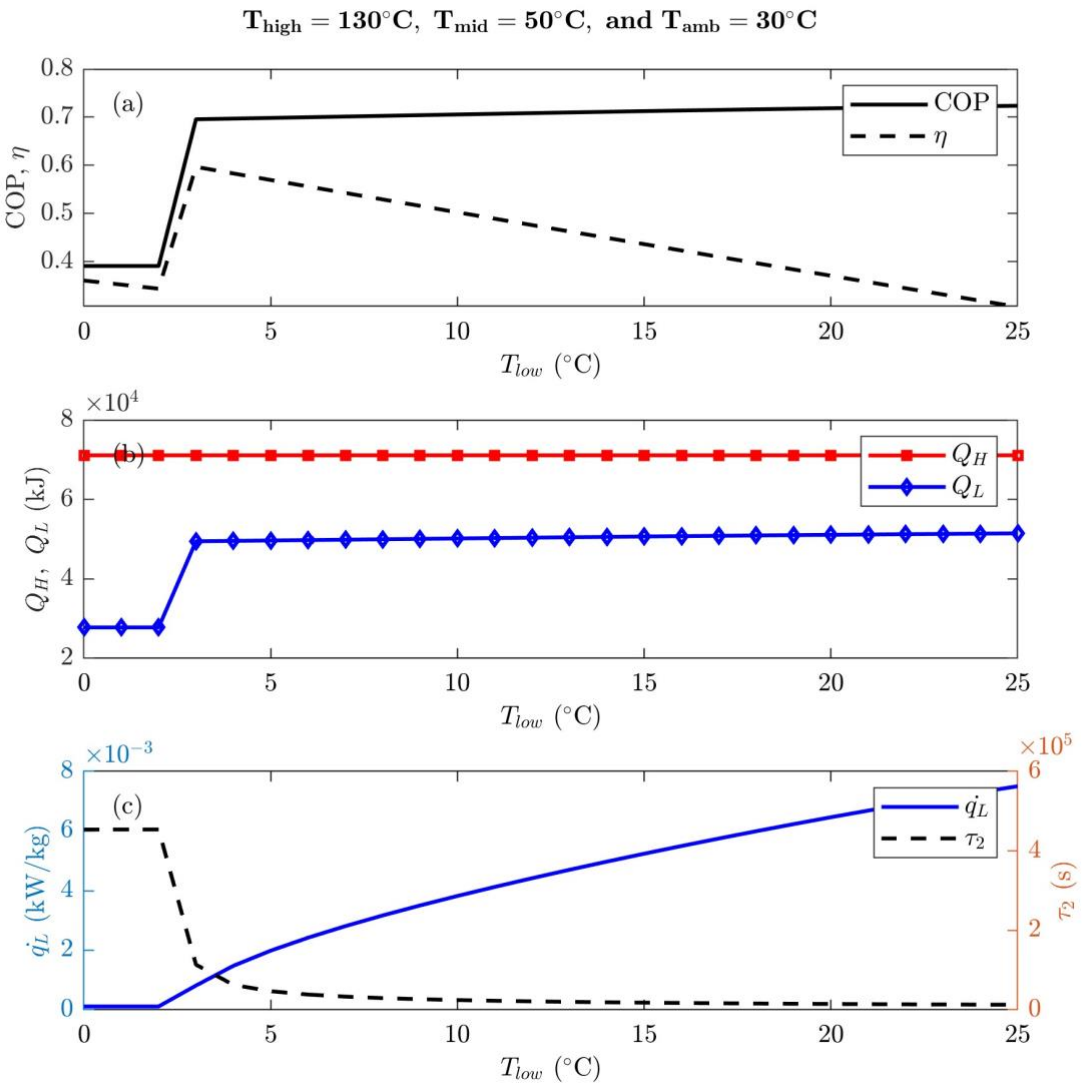


Fig. 10: Effect of low-temperature, $T_{low}$ for LTMH during the cooling cycle.

The effect of mid-temperature, $T_{mid}$ on the performance of the coupled MH system is shown in Fig. 11. It can be seen that an increase in $T_{mid}$ is detrimental to the specific power of the coupled MH system. During the regeneration cycle, an increase in $T_{mid}$ causes a decrease in the pressure gradient between HTMH and LTMH, which lowers the driving potential of hydrogen transfer from HTMH to LTMH. Similarly, during the cooling cycle, an increase in $T_{mid}$ causes decrease in the pressure gradient between LTMH and HTMH. Therefore, hydriding and dehydriding of LTMH occur at a slower rates, causing a decrease in $\dot{q}_H$ and $\dot{q}_L$, respectively as shown in Fig. 11(c). The COP is unaffected due to no change is overall values of total heat transferred to/from HTMH, $Q_H$ and LTMH, $Q_L$ respectively. The drastic fall in COP value at $T_{mid}$ of 60°C is due to a sharp decrease in $Q_L$ as shown in Fig. 11(b). It is because of poor hydrogen transfer potential from LTMH to HTMH under low pressure difference. However, the second law efficiency increases because of an increase in the sink temperature of the system as shown in Fig. 11(a). It can be noted that in a real system, the $T_{mid}$ temperature will depend on the HTF inlet temperature, which further may depend on the change in atmospheric (sink) conditions.

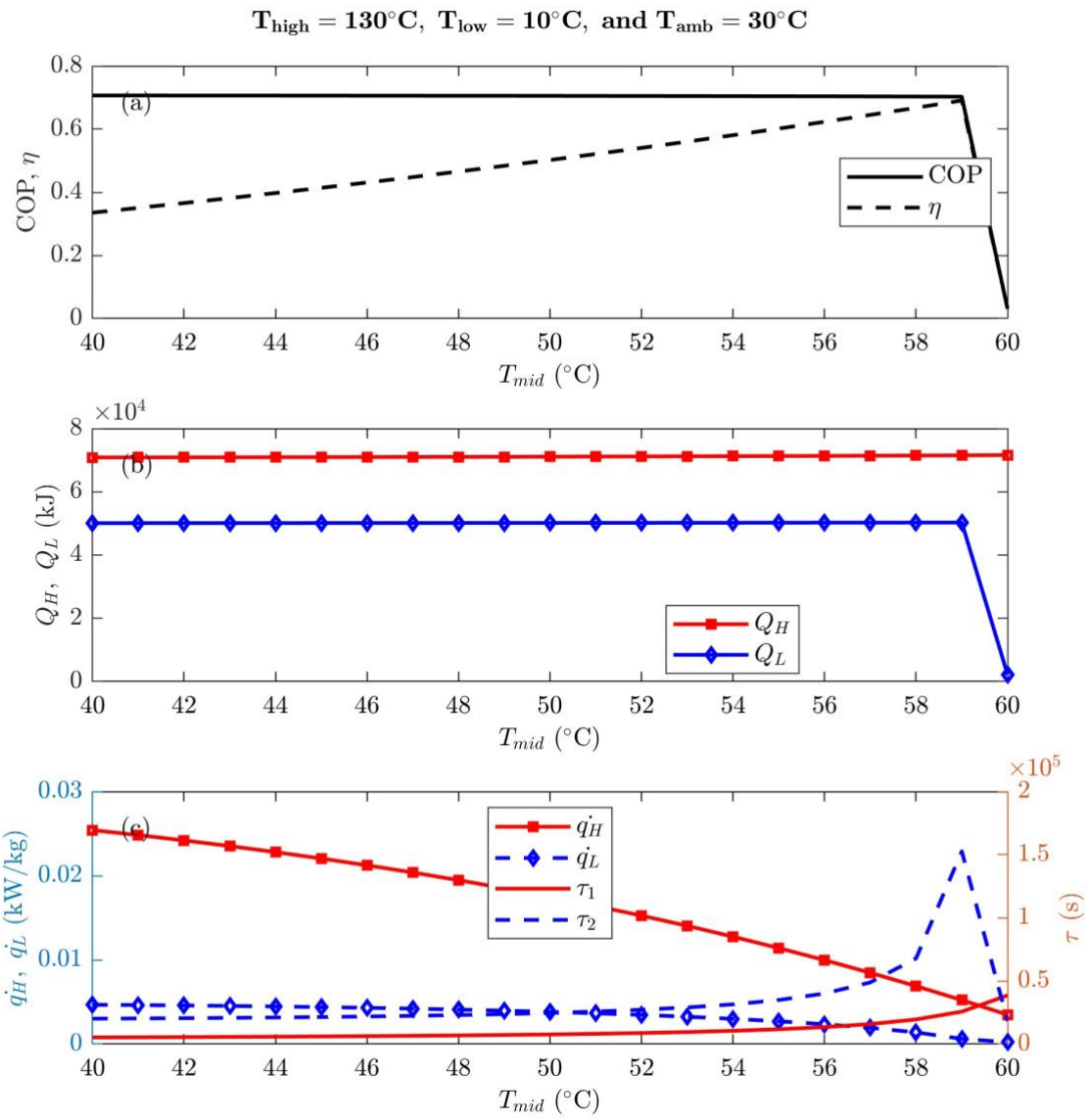


Fig. 11: Effect of mid-temperature, $T_{mid}$ on the performance of coupled MH system.

Typically, in a practical system, $T_{amb}$ would change with time if the system is designed to operate for fairly long durations. It is also subjected to change with seasons and the locations at which the system is operated. Therefore, it can be assumed that the MH system could be operating in a wide range of $T_{amb}$, and hence, its effect on the system performance is crucial. Furthermore, $T_{amb}$ defines the sink temperature for HTF in the MH system and, therefore, constrains the design for $T_{mid}$ and $T_{low}$. In the present system, an increase in $T_{amb}$ caused a decrease in the sensible heating load of HTMH and an increase in the sensible cooling load of LTMH during regeneration and cooling cycles, respectively. Therefore, both $Q_H$ and $Q_L$ decrease with an increase in $T_{amb}$ as shown in Fig. 12(b). Consequently, the COP of the system remains nearly constant, as shown in Fig. 12(a). On the other hand, the temperature difference between hydriding MHs and inlet HTF decreases with increased $T_{amb}$ causing an increase in

cycle time, as shown in Fig. 12(c). Furthermore, the effect of higher cycle time is shown in Fig. 12(c) that is reflected as lower specific power with high $T_{amb}$.

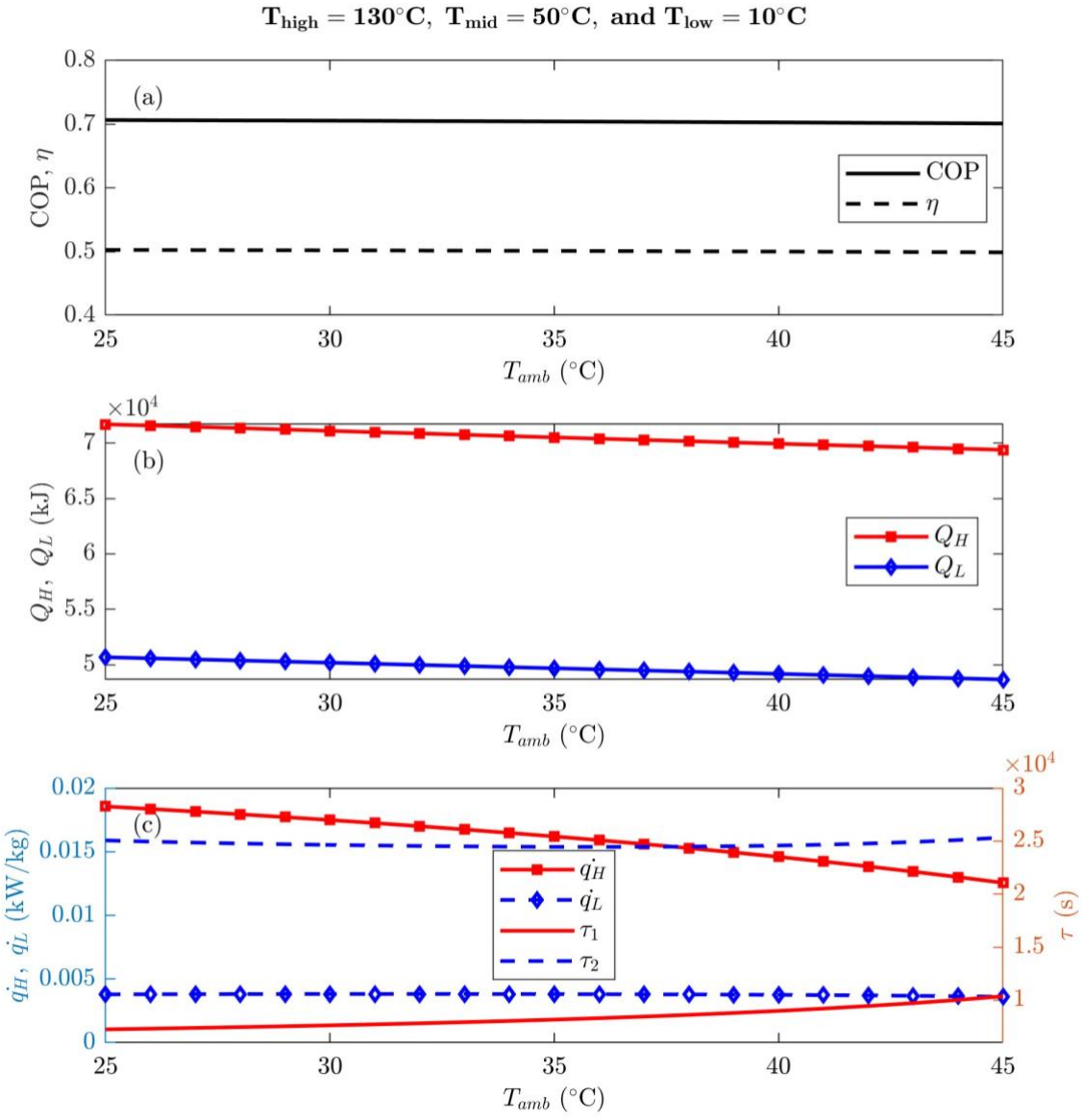


Fig. 12: Effect of ambient temperature, $T_{amb}$ on the performance of coupled MH system.

### 4.3 Effect of the control system

The effect of varying load demand on the coupled MH system is shown in Fig. 13 and Fig. 14, with a control system employed to regulate the hydrogen discharge rate. It is found that the designed control strategy is very effective for providing the cooling load demand. The control strategy was validated with two scenarios - scenario 1 considers a step signal for cooling demand, whereas scenario 2 considers the normalized form of an actual cooling demand from the building. In scenario 1, the load demand was varied in steps up to approximately 1000 W. The control loop 1 adjusts the required HTF flow rate for maintaining the temperature of hydride reactor at the given reference value. The HTF pump regulates the flow in the heat

exchanger based on the reference signal generated by the control loop 1. Therefore, an effective tracking of reference temperature is achieved in the hydride reactor. It can be observed that the hydrogen flow rate between the MH reactors is proportional to the cooling load demand, which is expected. A higher hydrogen flow rate between the MH reactors provides higher cooling. The proposed control loop 2 (in Fig. 5) effectively adjusts the values for reference hydrogen flow rate required for the cooling. It can be observed that the hydrogen flow rate remains within the minimum and maximum limits of approximately 0 and 4 g/s, respectively during the transient events of load variations. The minimum and maximum limits of a typical reactor will depend on the hydride type as well as the reactor design, which needs to be incorporated during the controller design. The variation in the temperature and pressure of MH reactors is shown in Fig. 13(c) and 13(d), respectively. The proposed control strategy maintains the temperature of HTMH and LTMH hydrides at given reference values. The value of the pressure in LTMH is higher than in high-temperature hydride, so it can discharge the required amount of hydrogen for cooling demand. In the transient events of load variations, the control loop 2 generates the reference hydrogen flow rate signal. Therefore, both control loops 2 and 3 function in coordination for facilitating the required cooling. Control loop 3 effectively adjusts the area of the control valve between MH reactors for regulating the reference hydrogen flow rate as shown in Fig. 13 and 14. Therefore, control loop 1 maintains the reference temperature of the hydrides while control loops 2 and 3 ensure the effective tracking of the cooling demand. As per the testing and validation of the controller in both scenarios, it is found that the controller is sufficient to meet the step as well as random variations in the cooling demand.

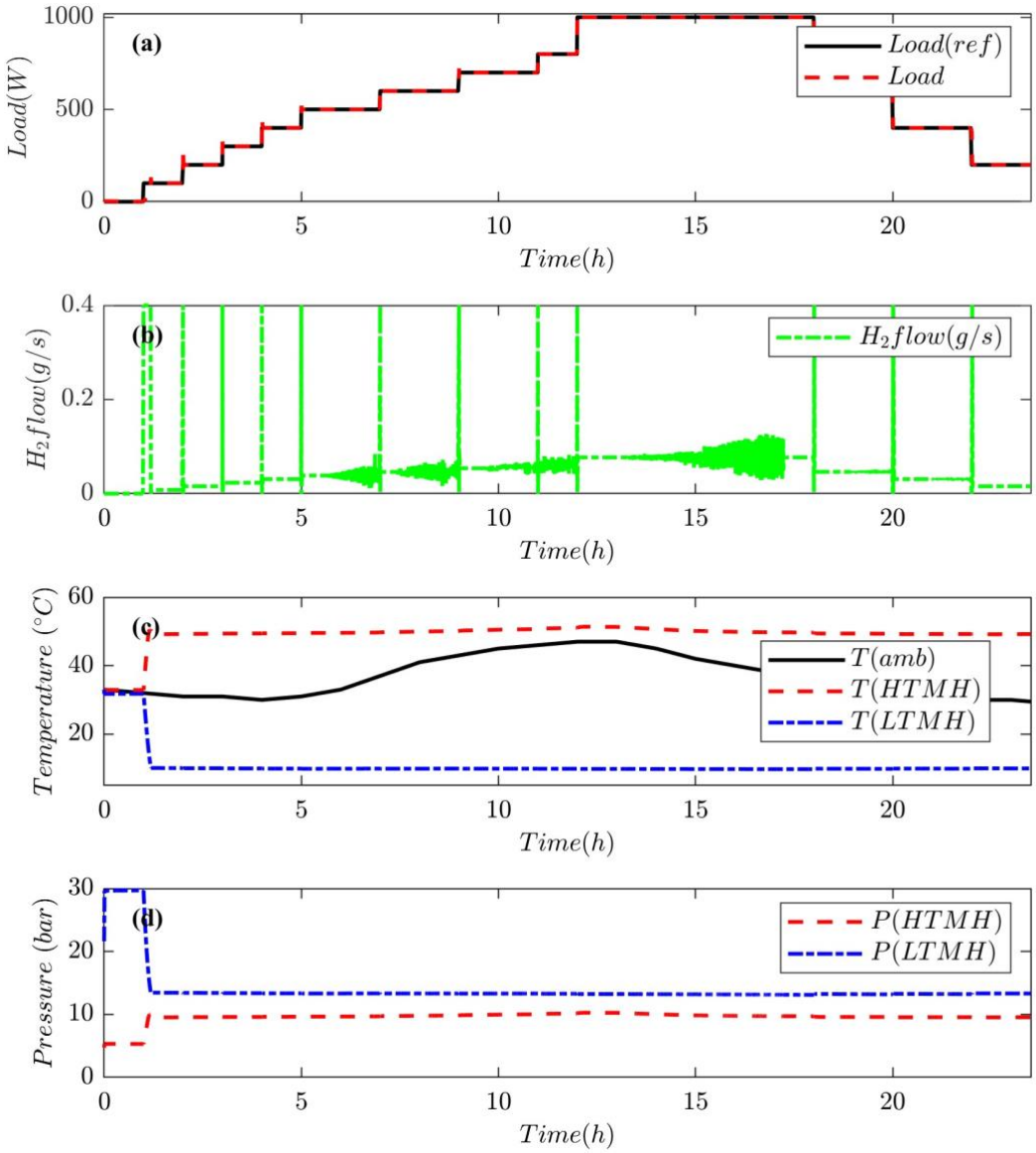


Fig. 13: Performance of proposed controller with a reference step signal (cooling load), (a) Tracking of reference and actual cooling load with time, (b) Variation of hydrogen flow rate with time, (c) Variation of MH reactor and ambient temperature with time, (d) Variation of MH reactor pressure with time.

Fig. 14(a) shows the reference cooling load and the coupled MH load response over one day. It can be seen that the control system is capable of regulating the hydrogen flow rate to meet the cooling load demand throughout the day, as shown in Fig. 14(b). Therefore, the coupled MH cooling load is closely following the reference cooling load with time. It can be noted that two pairs of such coupled MH systems can be adopted for continuous operation. In such a system, one pair operates in the cooling mode (discharge cycle), and other pair operates in the regeneration mode (charge cycle) as depicted in Fig. 1. At the end of the day, these MH pairs change their modes and consequently have the ability of providing a continuous operation. Furthermore, the dynamics and stability of the system can better be understood from Fig. 14(c) and Fig. 14(d), where the variations in temperature and pressure of the hydride

reactors are depicted, respectively. Fig. 14(c) shows the variation in ambient temperature along with both HTMH and LTMH reactor temperatures with time. Initially, the temperatures of both hydrides are the same, but the temperature of the HTMH is increased, and the LTMH is decreased gradually (due to thermal capacities) to their reference operating temperatures. This reference temperature tracking of hydride is achieved by the control loop 1. It can be seen that the system is capable of maintaining the constant hydride temperatures during the dynamic operation of the coupled MH system. The controller is found to maintain the mean reactor temperatures of 50.11℃ and 9.78℃ for HTMH and LTMH, respectively. It shows that the controller performance is adequately stable with standard deviations from reference values of 1.10℃ and 1.64℃ for HTMH and LTMH, respectively. It should be noted that the large difference of MH reference temperatures from ambient temperature (at the start) lead to slightly higher standard deviations. It can be observed that in scenario 2, the cooling load increases in smoother manner compared to the step variations in scenario 1, therefore, control loop 2 provides a slow variation in the hydrogen flow rate as compared to that of at scenario 1. The root mean square error (RMSE) between reference and actual cooling load is found as 5.78 W, which further reflect the accuracy and responsiveness of the designed controller. The pressure inside the hydride depends on the hydride temperature and amount of hydrogen stored. Therefore, the pressures of the coupled MH reactors remain nearly constant due to constant temperature operation of the hydride tank during the operation, as shown in Fig. 14(d). The controller is found to maintain the mean reactor pressures of 9.84 bar and 13.27 bar with standard deviations of 0.31 bar and 1.09 bar for HTMH and LTMH, respectively.

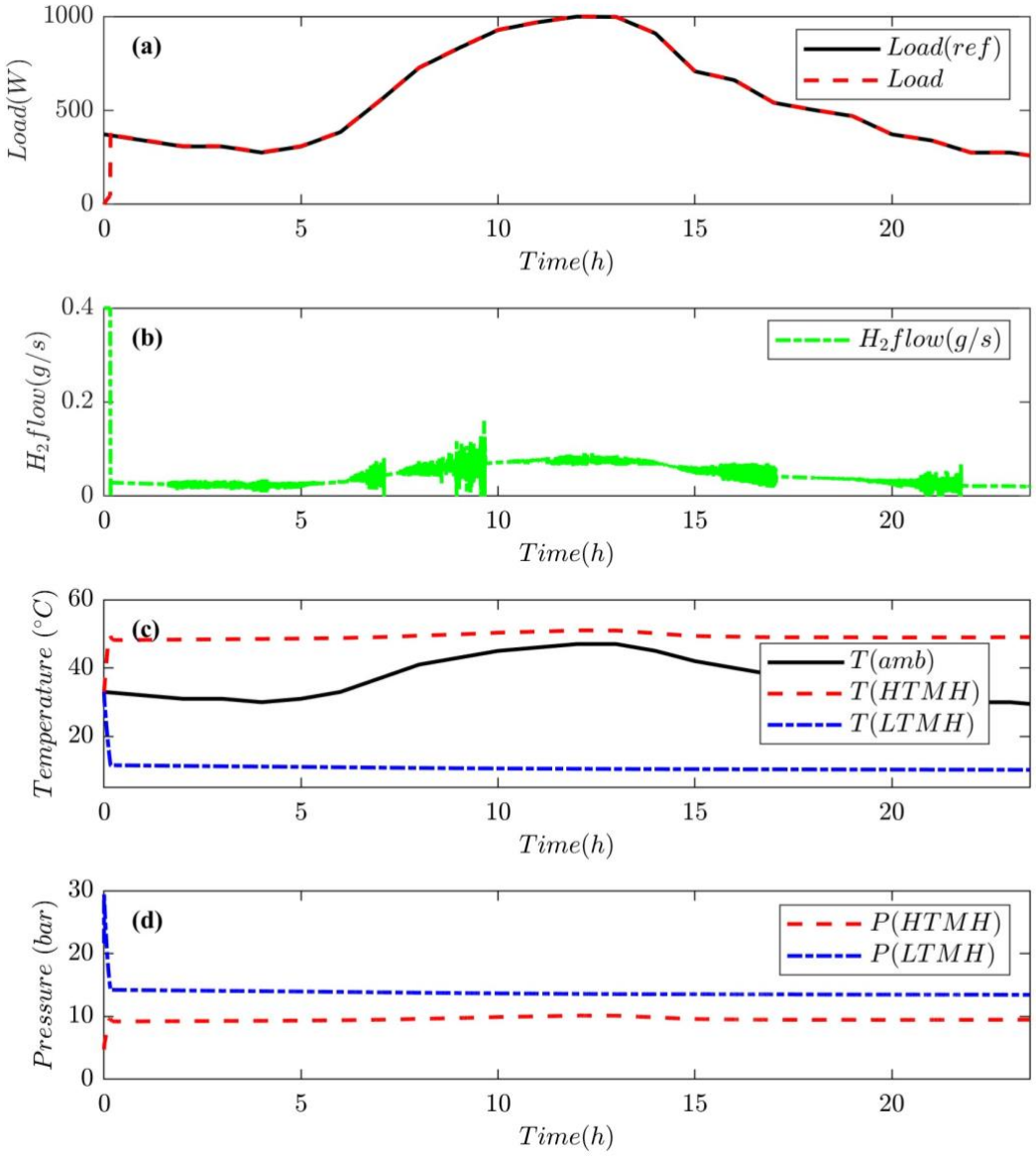


Fig. 14: Performance of proposed controller with a reference building load (cooling load), (a) Tracking of reference and actual cooling load with time, (b) Variation of hydrogen flow rate with time, (c) Variation of MH reactor and ambient temperature with time, (d) Variation of MH reactor pressure with time.

## 5. Conclusions

In the present work, a control-based dynamic modeling of a temperature-driven coupled MH cooling system is investigated to regulate the thermal demand in building applications. A thermochemical dynamic model of the temperature-driven coupled MH cooling system is created in MATLAB Simulink. The model is rigorously tested using numerous combinations of potential MH pairs, with an emphasis on identifying coupled MH systems that exhibit superior performance, as indicated by their high COP values. It is followed by a detailed parametric analysis to examine the impact of operational parameters, namely, $T_{high}$, $T_{low}$, $T_{mid}$, and $T_{amb}$. Finally, the study explores a control methodology to regulate the coupled MH

cooling system in response to the demand of a reference building cooling load. The main outcomes of the present study are summarized as follows:

- The selection of a hydride pair is a crucial step in the development of a temperature-driven coupled MH cooling system. There are a large number of potential hydride pairs, which necessitate the development of a simple selection model based on a few important criteria. A simple model is presented in the present study based on system COP values, where $Zr_{0.76}Ti_{0.24}Ni_{1.16}Mn_{0.63}V_{0.14}Fe_{0.18}$–$Ti_{0.85}Zr_{0.15}Cr_{1.2}Mn_{0.8}$ pair produced one of the highest COP of 0.71, and fastest reaction kinetics. In the future, a multi-criterion-based selection model can be developed using the target application-based weighted average method.

- Furthermore, a parametric investigation was performed to understand the effect of operating temperatures on the performance of the temperature-driven coupled MH cooling system. It was found that both high and low temperatures could be used to control the COP and specific power of the system. The system-specific power increased with an increase in high and low operating temperatures; however, the COP of the system showed an optimum value. There is a scope for the development of a control algorithm that optimizes the MH system COP and specific cooling power under the transient load demand. Furthermore, the middle temperature is found to be crucial, however, it is a restrictive parameter for the system performance control.

- Finally, a feedback controller was investigated to control the hydrogen flow between the coupled MH systems under a building transient load demand. It was found that the developed PI controller was capable of rejecting the signal noise from the hydrogen flow and internal heat exchange processes. The RMSE between the reference and actual cooling load was found as 5.78 W. Hence, the MH reactors were maintained at stable pressure and temperature conditions for continuous operation under a typical day transient building load demand.

Therefore, effective control is essential for the proper working of such a coupled MH based cooling system. Furthermore, there is a scope for integrating the proposed system with the conventional vapor compression refrigeration system for higher flexibility and reliability. Implementation of advanced control methods for such a system can be an interesting research proposal.

**Acknowledgment**

Authors would like to acknowledge the support of SERB, DST India, for supporting this work under SERB International Research Experience (SIRE) award number SIR/2022/000656. The research facility provided by National Renewable Energy Laboratory (NREL), CO, USA, is also gratefully acknowledged. Authors would like to recognize the encouragement and support of the Birla Institute of Technology and Science, Pilani (BITS Pilani) India, in carrying out this research work.

This work was authored in part by the National Renewable Energy Laboratory, operated by Alliance for Sustainable Energy, LLC, for the U.S. Department of Energy (DOE) under Contract No. DE-AC36-08GO28308. The views expressed in the article do not necessarily represent the views of the DOE or the U.S. Government. The U.S. Government retains and the publisher, by accepting the article for publication, acknowledges that the U.S. Government retains a nonexclusive, paid-up, irrevocable, worldwide license to publish or reproduce the published form of this work, or allow others to do so, for U.S. Government purposes.

**Nomenclature**

| | |
|---|---|
| $A$ | Arrhenius rate constant ($s^{-1}$) |
| $A_b$ | Available area of heat transfer of cooling space ($m^2$) |
| $A_c$ | Cross-sectional area of the connecting pipe ($m^2$) |
| $A_{HTF}$ | Available area of heat transfer of heat transfer fluid ($m^2$) |
| $C_v$ | Flow coefficient of the control valve |
| $C_p$ | Specific heat capacity (J $kg^{-1}$ $K^{-1}$) |
| $COP$ | Coefficient of performance |
| $COP_{rev}$ | Ideal coefficient of performance |
| $E$ | Activation energy for hydrogen absorption or desorption (J $mol^{-1}$) |
| $G_{PI,i}$ | PI control loop |
| $G_{0,i}$ | Plant equation |
| $\Delta H$ | Change in enthalpy for hydrogen absorption or desorption (J $mol^{-1}$) |
| $k$ | Material thermal conductivity (W/m.K) |
| $M_{H_2}$ | Molar mass of hydrogen (kg $mol^{-1}$) |
| $\dot{m}_{H_2}$ | Mass flow rate of hydrogen (kg $s^{-1}$) |
| $\dot{m}_{HTF}$ | Mass flow rate of heat transfer fluid (kg $s^{-1}$) |
| $m_{HTMH}$ | Mass of high-temperature metal hydride (kg) |
| $m_{LTMH}$ | Mass of low-temperature metal hydride (kg) |
| $n$ | Order of reaction for hydrogen absorption or desorption |
| $P$ | Pressure of the hydride (Pa) |
| $P_0$ | Atmospheric pressure (Pa) |
| $P_{eq}$ | Equilibrium pressure of the hydride (Pa) |
| $\dot{q}_H$ | Specific heating power (W $kg^{-1}$) |
| $\dot{q}_L$ | Specific cooling power (W $kg^{-1}$) |
| $Q_H$ | Heat input in the regeneration cycle (J) |
| $Q_L$ | Cooling output in the cooling cycle (J) |
| $\dot{Q}_{IHG}$ | Internal heat gain (W) |
| $\dot{Q}_{SHG}$ | Solar heat gain (W) |
| $R$ | Ideal gas constant (J $mol^{-1}$ $K^{-1}$) |
| $\Delta S$ | Change in entropy for hydrogen absorption or desorption (J $mol^{-1}$ $K^{-1}$) |
| $T_{hyd}$ | Temperature of the hydride (K) |
| $T_{high}$ | High temperature of the metal hydride system (K) |
| $T_{mid}$ | Middle temperature of the metal hydride system (K) |
| $T_{low}$ | Low temperature of the metal hydride system (K) |
| $T_{amb}$ | Ambient temperature (K) |
| $T_{set}$ | Target comfort temperature (K) |

| | |
|---|---|
| $U_b$ | Overall heat transfer coefficient of cooling space (W m$^{-2}$ K$^{-1}$) |
| $U_{HTF}$ | Overall heat transfer coefficient of heat transfer fluid (W m$^{-2}$ K$^{-1}$) |
| $V_{H_2}$ | Initial storage volume in hydride (m$^3$) |
| $w$ | Mass fraction of hydrogen stored in the hydride |
| $w_{max}$ | Maximum mass fraction capacity of the hydride |
| $x_{LTMH}$, and $x_{HTMH}$ | Equilibrium point in the hydrogen transfer |
| **Greek Letters** | |
| $\eta_{hyd}$ | Hydriding efficiency (%) |
| $\eta$ | Second law efficiency (%) |
| $\tau_1$ | Regeneration cycle time (s) |
| $\tau_2$ | Cooling cycle time (s) |
| ρ | Material crystal density (kg/m$^3$) |
| $\rho_{H_2}$ | Hydrogen density (kg/m$^3$) |
| **Subscripts** | |
| 0 | Reference condition |
| amb | Ambient |
| eq | Equilibrium |
| $H_2$ | Hydrogen |
| hyd | Hydride |
| IHG | Internal heat gain |
| in | Inlet condition |
| max | Maximum |
| out | Outlet condition |
| ref | Reference |
| rev | Reversible |
| set | Set condition |
| SHG | Solar heat gain |
| **Abbreviations** | |
| ADRC | Active disturbance rejection control |
| CES | Chemical energy storage |
| COP | Coefficient of performance |
| CSP | Concentrated solar power |
| ECES | Electrochemical energy storage |
| EES | Electrical energy storage |
| GHI | Global horizontal irradiation |
| HTMH | High-temperature metal hydride |
| HVAC | Heating ventilation and air conditioning |
| HX | Heat exchanger |
| LHS | Latent heat storage |
| LTMH | Low-temperature metal hydride |
| MES | Mechanical energy storage |
| ODEs | Ordinary differential equations |
| PCM | Phase change material |
| PCT | Pressure-composition-temperature |

| | |
|---|---|
| PI | Proportional-integral |
| RMSE | Root mean square error |
| SCP | Specific cooling power |
| SHS | Sensible heat storage |
| TCES | Thermochemical energy storage |
| TES | Thermal energy storage |

**Appendix A.**

Table A.1: Comparison between metal hydride (MH) and phase change material (PCM) based thermal energy storage for building applications. [3, 4, 46, 47, 49, 50, 51]

| **Parameters** | **Metal Hydride TES** | **Phase Change Material (PCM) TES** |
|---|---|---|
| Storage mechanism | Hydrogen absorption/desorption | Phase transition |
| Self-discharge rate | Low (months) | High (days to weeks, especially for organic PCMs) |
| Gravimetric energy density (kJ/kg) | 360-600 | 100-300 |
| Volumetric energy density ($GJ/m^3$) | 0.5-3 | 0.1-0.3 |
| Operating temperature range (°C) | Wide range of operation and high flexibility (-50 to 200) | Less flexibility due to fixed transition temperature of PCM (-50 to 150) |
| Charging/discharging rate | Fast (1–30 minutes) | Moderate (1–10 hours) |
| Thermal conductivity (W/mK) | 10-50 | 0.1-1 |
| Cycling stability | Higher (>10,000 cycles) | Lower (1,000-5,000 cycles) |
| Safety concerns | Hydrogen leakage | Phase segregation, and super cooling |
| Cost ($/kWh) | Higher (100-200) | Lower (50-100) |
| Integration with building | More complex integration, may requires specialized equipment | Easier integration and retrofitting |

## Appendix B. Model description

### B.1 Kinetics model

The rate of change of mass fraction of hydrogen stored in the MH can be expressed as the product of an Arrhenius rate equation, a pressure limiting function, and a function that depends on reaction order [52]:

$$\frac{dw}{dt} = A.\exp\left(\frac{-E}{RT}\right).\ln\left(\frac{P}{P_{eq}}\right).w_{max}.\left(\frac{w}{w_{max}} - i\right)^{n} \quad \text{(B.1)}$$

$$i = \begin{cases} 0, & P \leq P_{eq} \\ 1, & P > P_{eq} \end{cases}$$

where $w$ is the mass fraction of hydrogen stored in the hydride and $dw/dt$ is the time rate of hydrogen absorption/desorption in/from the MH. The direction of the reaction depends on the pressure, $P$ of the MH at a given temperature, $T$. The absorption of hydrogen in the MH takes place if the operating pressure is higher than the equilibrium pressure, $P_{eq}$ a given temperature, $T$. $w_{max}$ represents the maximum mass fraction capacity of the hydride. The constants Arrhenius rate, $A$, activation energy, $E$, gas constant, $R$, and the order of reaction, $n$ depend on the hydride material.

A reliable and accurate estimation of the equilibrium pressure is required to model the dynamic temperature response of an MH reactor accurately. It can be achieved using a suitable PCT model for the MH that describes the equilibrium pressure variation with the hydrogen concentration, and temperature. However, PCT models for all the hydrides are unavailable in the toolbox. Furthermore, using PCT models to extract equilibrium pressure is a tedious task, and hence unsuitable for the present work that compares a large number of hydride pairs. Therefore, Van't Hoff equation is used to acquire the equilibrium pressures, which is a simpler approach however gives reasonably accurate estimations. The isotherms of PCT model are divided into α, α + β, and β regions; pressure remains relatively constant as the hydrogen concentration increases in the two-phase region (α + β), which is also known as plateau region. The MH pair is assumed to be operating in the α + β region, where the equilibrium pressure is given by Van't Hoff equation:

$$\ln\left(\frac{P_{eq}}{P_0}\right) = \frac{\Delta H}{RT} - \frac{\Delta S}{R} \quad \text{(B.2)}$$

where $P_0$ is the reference pressure that is atmospheric in the present work. $\Delta H$ and $\Delta S$ are the changes in enthalpy and entropy of the chemical reaction for the given metal hydride. It can be noted that the effect of hysteresis is important in the charging and discharging of MH systems [53], which may considerably affect the system performance.

**B.2 Thermodynamic model**

A thermodynamic model of the hydride pair was established to obtain the evolution of temperature and pressure inside the hydride reactors. The energy balance for the system was used to calculate the rate of change in hydride temperature ($dT_{hyd}/dt$) as shown below:

$$\left(mC_p\right)_{hyd}.\frac{dT_{hyd}}{dt} = \left(\frac{m_{hyd}}{M_{H_2}}.\frac{dw}{dt}.\Delta H\right) + \left(\dot{m}C_p\right)_{H_2}.(T_{in} - T_{out})_{H_2} + \left(\dot{m}C_p\right)_{HTF}.(T_{in} - T_{out})_{HTF} \quad \text{(B.3)}$$

where $m$ and $\dot{m}$ show mass and mass flow rates, respectively of various species. $C_p$ shows specific heat at constant pressure, and $M_{H_2}$ shows the molecular mass of hydrogen. The first term on the right side of the equation represents the heat released/adsorbed by the hydride in the reaction. The second term represents energy transfer by hydrogen mass transfer. The third term represents energy transfer by the heat transfer fluid (HTF).

In this work, an MH core is designed in the cylindrical shape carrying an internal heat exchanger consisting of a concentric cooling tube to improve the heat transfer between the MH core and the coolant. The method developed by Corgnale et al. [54] was used to estimate the sizing of the MH core to deliver the required amount of hydrogen. It was assumed that the minimum charging time required for the MH is one hour, and the maximum temperature difference between the inner and outer surfaces is limited to 10°C. Thereafter, the characteristic length can be calculated based on the properties of the MH. In this work, the adiabatic boundary condition at the outer surface of the MH core is considered under cylindrical coordinates; a detailed description of the design methodology can be found in Corgnale et al. [54]. In this work, a single MH core is designed with a diameter of 3.2 cm (1.259 inch), having an HTF tube of an outer diameter of 0.8 cm (0.315 inch) and an inner diameter of 0.7 cm (0.276 inch) at the center. The MH reactor is composed of a collection of such MH cores. The material of the HTF tube is aluminum, and the thermal resistance of the tube is assumed to be small compared to the MH and HTF. The outlet temperature of the HTF is calculated as:

$$T_{out} - T_{hyd} = \left(T_{in} - T_{hyd}\right).\exp\left(\frac{-(UA)_{HTF}}{\left(\dot{m}C_p\right)_{HTF}}\right) \quad \text{(B.4)}$$

where $U_{HTF}$ and $A_{HTF}$ show the overall heat transfer coefficient between the HTF and hydride, and the available area of heat transfer, respectively. The approach used by Kumar et al. [55] is employed to calculate the overall heat transfer coefficient. The HTFs are Paratherm oil and 50% (v/v) Ethylene glycol/water for HTMH and LTMH, respectively. Finally, the cooling load ($\dot{Q}_L$) for the MH can be calculated as:

$$\dot{Q}_L = \left(\dot{m}C_p\right)_{HTF}.(T_{in} - T_{out})_{HTF} \quad \text{(B.5)}$$

The mass flow rate of hydrogen, $\dot{m}_{H_2}$ can be calculated by considering the flow of hydrogen through a connecting pipe between the hydride reactors as follows:

$$\dot{m}_{H_2} = C_v A_c \sqrt{2.\rho_{H_2}.(P_{LTMH} - P_{HTMH})} \quad \text{(B.6)}$$

where $C_v$ is the flow coefficient of the control valve, $A_c$ is the cross-sectional area of the connecting pipe, and $\rho_{H_2}$ is the density of hydrogen. $P_{LTMH}$ and $P_{HTMH}$ are the pressures of hydride reactors LTMH and HTMH, respectively. A positive pressure difference is required for the net flow of hydrogen, which also sets the direction of flow in the equation. The pressures of the reactors are established by employing a mass balance equation, which connects the changes in hydrogen mass to the reaction rate and the hydrogen flow rate. The total mass of hydrogen in the coupled MH system is taken as 5 kg, which was found sufficient to provide the cooling effect according to the load profile considered in the present work. Then, the mass balance for hydrogen in the gaseous phase in the rate terms can be written as:

$$\frac{dm_{H_2}}{dt} = \left(m_{hyd}.\frac{dw}{dt}\right) \pm \dot{m}_{H_2} \quad \text{(B.7)}$$

The change in pressure over time depends on the alterations in mass and temperature in the hydride reactors. Assuming that the gaseous hydrogen follows the ideal gas equation, it can be written in the form of a differential equation as follows:

$$\frac{dP}{dt} = \frac{RT}{V_{H_2}}.\frac{dm_{H_2}}{dt} \quad \text{(B.8)}$$

where $V_{H_2}$ is the initial volume available for the storage of hydrogen in the hydride. It can be noted that the instantaneous temperature of the hydride reactor is taken in the calculation, and hydrogen temperature is assumed to be equal to the instantaneous reactor temperature.

## References


1. Desai F, Prasad JS, Muthukumar P, Rahman MM. Thermochemical energy storage system for cooling and process heating applications: A review. Energy Conversion and Management. 2021 Feb 1;229:113617. https://doi.org/10.1016/j.enconman.2020.113617

2. Li G, Zheng X. Thermal energy storage system integration forms for a sustainable future. Renewable and Sustainable Energy Reviews. 2016 Sep 1;62:736-57. https://doi.org/10.1016/j.rser.2016.04.076

3. Kishore RA, Bianchi MV, Booten C, Vidal J, Jackson R. Modulating thermal load through lightweight residential building walls using thermal energy storage and controlled precooling strategy. Applied Thermal Engineering. 2020 Nov 5;180:115870. https://doi.org/10.1016/j.applthermaleng.2020.115870

4. Kishore RA, Bianchi MV, Booten C, Vidal J, Jackson R. Parametric and sensitivity analysis of a PCM-integrated wall for optimal thermal load modulation in lightweight

buildings. Applied Thermal Engineering. 2021 Mar 25;187:116568. https://doi.org/10.1016/j.applthermaleng.2021.116568

5. Alva G, Lin Y, Fang G. An overview of thermal energy storage systems. Energy. 2018 Feb 1;144:341-78. https://doi.org/10.1016/j.energy.2017.12.037

6. Abdin Z, Webb CJ, Gray EM. One-dimensional metal-hydride tank model and simulation in Matlab–Simulink. International Journal of Hydrogen Energy. 2018 Mar 8;43(10):5048-67. https://doi.org/10.1016/j.ijhydene.2018.01.100

7. H Abedin A, A Rosen M. A critical review of thermochemical energy storage systems. The open renewable energy journal. 2011 Aug 9;4(1). http://dx.doi.org/10.2174/1876387101004010042

8. Manickam K, Mistry P, Walker G, Grant D, Buckley CE, Humphries TD, Paskevicius M, Jensen T, Albert R, Peinecke K, Felderhoff M. Future perspectives of thermal energy storage with metal hydrides. International Journal of Hydrogen Energy. 2019 Mar 22;44(15):7738-45. https://doi.org/10.1016/j.ijhydene.2018.12.011

9. Kumar S, Dutta P, Murthy SS, Aristov YI, Gordeeva L, Li TX, Wang RZ. Studies on a metal hydride based year-round comfort heating and cooling system for extreme climates. Energy and Buildings. 2021 Aug 1;244:111042. https://doi.org/10.1016/j.enbuild.2021.111042
10. Krane P, Ziviani D, Braun JE, Jain N, Marconnet A. Techno-economic analysis of metal-hydride energy storage to enable year-round load-shifting for residential heat pumps. Energy and Buildings. 2022 Feb 1;256:111700. https://doi.org/10.1016/j.enbuild.2021.111700

11. Paskevicius M, Sheppard DA, Williamson K, Buckley CE. Metal hydride thermal heat storage prototype for concentrating solar thermal power. Energy. 2015 Aug 1;88:469-77. https://doi.org/10.1016/j.energy.2015.05.068

12. Dornheim M. Thermodynamics of metal hydrides: tailoring reaction enthalpies of hydrogen storage materials. In Thermodynamics-Interaction Studies-Solids, Liquids and Gases 2011 Nov 2. IntechOpen. DOI: 10.5772/21662

13. Linder M, Mertz R, Laurien E. Experimental results of a compact thermally driven cooling system based on metal hydrides. International Journal of Hydrogen Energy. 2010 Jul 1;35(14):7623-32. https://doi.org/10.1016/j.ijhydene.2010.04.184

14. Kölbig M, Bürger I, Linder M. Thermal applications in vehicles using Hydralloy C5 in single and coupled metal hydride systems. Applied Energy. 2021 Apr 1;287:116534. https://doi.org/10.1016/j.apenergy.2021.116534

15. Ge YT, Lang PY. Performance analysis of a metal hydride refrigeration system.

Applied Thermal Engineering. 2023 Nov 5;234:121264. https://doi.org/10.1016/j.applthermaleng.2023.121264

16. M. Mohan, S. Maitray, V.K. Sharma, E. Anil Kumar, A. Satheesh, P. Muthukumar. Performance analysis of metal hydride based simultaneous cooling and heat transformation system. Int. J. Hydrogen Energy, 44 (2019), pp. 10906-10915, https://doi.org/10.1016/j.ijhydene.2019.02.241

17. Choudhari M, Ahuja K, Thakkur S, Bardhan S, Sharma VK. Performance investigation of metal hydride based heat transformer. Energy Storage. 2019 Apr;1(2):e56. https://doi.org/10.1002/est2.56

18. Ge YT, Lang PY. Alloy selections in high-temperature metal hydride heat pump systems for industrial waste heat recovery. Energy Reports. 2022 Nov 1;8:3649-60. https://doi.org/10.1016/j.egyr.2022.02.279

19. Wimmer A, Linder M, Bürger I. Lumped model for a quasi-continuously operating open metal hydride heat pump system. Applied Thermal Engineering. 2024 Mar 15;241:122250. https://doi.org/10.1016/j.applthermaleng.2023.122250

20. Gruen DM, Mendelsohn MH, Sheft I. Metal hydrides as chemical heat pumps. Solar Energy. 1978 Jan;21(2):153-6. https://doi.org/10.1016/0038-092X(78)90043-9

21. Ron M. A hydrogen heat pump as a bus air conditioner. Journal of the Less Common Metals. 1984 Dec 17;104(2):259-78. https://doi.org/10.1016/0022-5088(84)90411-9

22. Golben PM, Huston EL. Design and fabricate a metallic-hydride heat pump with a cooling capacity of 9000 Btu/h. Final report. ERGENICS, Wyckoff, NJ (USA); 1989 Feb 7. https://www.osti.gov/biblio/5110718

23. Weckerle C, Bürger I, Linder M. Novel reactor design for metal hydride cooling systems. International Journal of Hydrogen Energy. 2017 Mar 23;42(12):8063-74. https://doi.org/10.1016/j.ijhydene.2017.01.066

24. Chandrakala B, Babu KS, Kumar EA. Thermodynamic analysis of La and Mm based metal hydride pairs for solar energy-driven cold storage applications. Thermal Science and Engineering Progress. 2024 May 1;50:102548. https://doi.org/10.1016/j.tsep.2024.102548

25. Zohra FT, Webb CJ, Lamb KE, Gray EM. Degradation of metal hydrides in hydrogen-based thermodynamic machines: a review. International Journal of Hydrogen Energy. 2024 Apr 25;64:417-38. 10.1016/j.ijhydene.2024.03.228

26. Muthukumar P, Kumar A, Raju NN, Malleswararao K, Rahman MM. A critical review on design aspects and developmental status of metal hydride based thermal machines. international journal of hydrogen energy. 2018 Sep 13;43(37):17753-79. https://doi.org/10.1016/j.ijhydene.2018.07.157

27. Gkanas EI, Khzouz M, Panagakos G, Statheros T, Mihalakakou G, Siasos GI, Skodras G, Makridis SS. Hydrogenation behavior in rectangular metal hydride tanks under effective heat management processes for green building applications. Energy. 2018 Jan 1;142:518-30. https://doi.org/10.1016/j.energy.2017.10.040

28. Tange M, Maeda T, Nakano A, Ito H, Kawakami Y, Masuda M, Takahashi T. Experimental study of hydrogen storage with reaction heat recovery using metal hydride in a totalized hydrogen energy utilization system. International Journal of Hydrogen Energy. 2011 Sep 1;36(18):11767-76. https://doi.org/10.1016/j.ijhydene.2011.06.023

29. Zhong Y, Glanville P. Metal-hydride adsorption systems for space conditioning in commercial and residential buildings. In ASME International Mechanical Engineering Congress and Exposition 2014 Nov 14 (Vol. 46552, p. V08AT10A080). American Society of Mechanical Engineers. https://doi.org/10.1115/IMECE2014-39943

30. Paya J, Linder M, Laurien E, Corberan JM. Dynamic model and experimental results of a thermally driven metal hydride cooling system. International journal of hydrogen energy. 2009 Apr 1;34(7):3173-84. https://doi.org/10.1016/j.ijhydene.2009.01.085

31. Payá J, Linder M, Mertz R, Corberán JM. Analysis and optimization of a metal hydride cooling system. International Journal of Hydrogen Energy. 2011 Jan 1;36(1):920-30. https://doi.org/10.1016/j.ijhydene.2010.08.112

32. Satheesh A, Muthukumar P, Dewan A. Computational study of metal hydride cooling system. International journal of hydrogen energy. 2009 Apr 1;34(7):3164-72. https://doi.org/10.1016/j.ijhydene.2009.01.083

33. Mellouli S, Askri F, Dhaou H, Jemni A, Nasrallah SB. Parametric studies on a metal-hydride cooling system. International journal of hydrogen energy. 2009 May 1;34(9):3945-52. https://doi.org/10.1016/j.ijhydene.2009.03.010

34. Nyamsi SN, Tolj I. The impact of active and passive thermal management on the energy storage efficiency of metal hydride pairs based heat storage. Energies. 2021 May 22;14(11):3006. https://doi.org/10.3390/en14113006

35. Cho JH, Yu SS, Kim MY, Kang SG, Lee YD, Ahn KY, Ji HJ. Dynamic modeling and simulation of hydrogen supply capacity from a metal hydride tank. International journal of hydrogen energy. 2013 Jul 17;38(21):8813-28. https://doi.org/10.1016/j.ijhydene.2013.02.142

36. Aruna R, Christa SJ. Modeling, system identification and design of fuzzy PID controller for discharge dynamics of metal hydride hydrogen storage bed. International Journal of Hydrogen Energy. 2020 Feb 7;45(7):4703-19. https://doi.org/10.1016/j.ijhydene.2019.11.238

37. Krane P, Nash AL, Ziviani D, Braun JE, Marconnet AM, Jain N. Dynamic modeling and control of a two-reactor metal hydride energy storage system. Applied Energy. 2022 Nov 1;325:119836. https://doi.org/10.1016/j.apenergy.2022.119836

38. Keow AL, Mayhall A, Cescon M, Chen Z. Active disturbance rejection control of metal hydride hydrogen storage. International Journal of Hydrogen Energy. 2021 Jan 1;46(1):837-51. https://doi.org/10.1016/j.ijhydene.2020.09.169

39. Nasrallah SB, Jemni A. Heat and mass transfer models in metal-hydrogen reactor. International Journal of Hydrogen Energy. 1997 Jan 1;22(1):67-76. https://doi.org/10.1016/S0360-3199(96)00039-0

40. Waters EL, Pourpoint TL, Voskuilen TG. Metal Hydride Component Design (MHy-CoDe) Tool for the Selection of Hydrides in Thermal Systems. 32nd International Thermal Conductivity Conference, 20th International Thermal Expansion Symposium, April 27–May 1, 2014, Purdue University, West Lafayette, Indiana, USA. https://core.ac.uk/download/77942872.pdf. DOI: 10.5703/1288284315541

41. Voskuilen TG, Waters EL, Pourpoint TL. A comprehensive approach for alloy selection in metal hydride thermal systems. International journal of hydrogen energy. 2014 Aug 22;39(25):13240-54. https://doi.org/10.1016/j.ijhydene.2014.06.119

42. Purdue Metal Hydride Toolbox. https://github.com/PurdueH2Lab/MetalHydrideToolbox

43. Bequette BW. Process control: modeling, design, and simulation. Prentice Hall Professional; 2003.

44. Arora, C.P. Refrigeration and Air Conditioning. Third Edition, Tata McGraw-Hill, 2009.

45. Gopal MR, Murthy SS. Experiments on a metal hydride cooling system working with ZrMnFe/MmNi4. 5Al0. 5 pair. International journal of refrigeration. 1999 Mar 1;22(2):137-49. https://doi.org/10.1016/S0140-7007(98)00033-4

46. Muthukumar P, Groll M. Metal hydride based heating and cooling systems: a review. International journal of Hydrogen Energy. 2010 Aug 1;35(16):8816-29. https://doi.org/10.1016/j.ijhydene.2010.01.115

47. Malleswararao K, Dutta P. Applications of metal hydride based thermal systems: A review. Applied Thermal Engineering. 2022 Oct 1;215:118816. https://doi.org/10.1016/j.applthermaleng.2022.118816

48. Hariyadi A, Suwarno S, Denys RV, von Colbe JB, Sætre TO, Yartys V. Modeling of the hydrogen sorption kinetics in an AB2 laves type metal hydride alloy. Journal of

Alloys and Compounds. 2022 Feb 10;893:162135. https://doi.org/10.1016/j.jallcom.2021.162135

49. Kurdi A, Almoatham N, Mirza M, Ballweg T, Alkahlan B. Potential phase change materials in building wall construction—a review. Materials. 2021 Sep 15;14(18):5328. **https://doi.org/10.3390/ma14185328**

50. Sarbu I, Sebarchievici C. A comprehensive review of thermal energy storage. Sustainability. 2018 Jan 14;10(1):191. **https://doi.org/10.3390/su10010191**

51. Modi P, Aguey-Zinsou KF. Room temperature metal hydrides for stationary and heat storage applications: a review. Frontiers in Energy Research. 2021 Apr 9;9:616115. https://doi.org/10.3389/fenrg.2021.616115

52. Wijayanta AT, Nakaso K, Aoki T, Kitazato Y, Fukai J. Effect of pressure, composition and temperature characteristics on thermal response and overall reaction rates in a metal hydride tank. International journal of hydrogen energy. 2011 Mar 1;36(5):3529-36. https://doi.org/10.1016/j.ijhydene.2010.12.047

53. Qian S, Northwood DO. Hysteresis in metal-hydrogen systems: a critical review of the experimental observations and theoretical models. International journal of hydrogen energy. 1988 Jan 1;13(1):25-35. https://doi.org/10.1016/0360-3199(88)90006-7

54. Corgnale C, Hardy BJ, Tamburello DA, Garrison SL, Anton DL. Acceptability envelope for metal hydride-based hydrogen storage systems. International journal of hydrogen energy. 2012 Feb 1;37(3):2812-24. https://doi.org/10.1016/j.ijhydene.2011.07.037

55. Kumar K, Alam M, Verma S, Dutta V. Analysis of metal hydride storage on the basis of thermophysical properties and its application in microgrid. Energy Conversion and Management. 2020 Oct 15;222:113217. https://doi.org/10.1016/j.enconman.2020.113217